

THS 1 375 9202

This is to certify that the thesis entitled

A UNIFIED MOMENTUM EQUATION APPROACH FOR FLUID-STRUCTURE INTERACTION (FSI) PROBLEMS WITH STATIONARY BOUNDARIES

presented by

Jagadish Gattu

has been accepted towards fulfillment of the requirements for the

M.S.	_ degree in	Mechanical Engineering
	K, 1	Yenn
	Major Pro	fessor's Signature
		05-09-05
		Date

MSU is an Affirmative Action/Equal Opportunity Institution

LIBRARIES MICHIGAN STATE UNIVERSITY EAST LANSING, MICH 48824-1048 PLACE IN RETURN BOX to remove this checkout from your record.

TO AVOID FINES return on or before date due.

MAY BE RECALLED with earlier due date if requested.

DATE DUE	DATE DUE	DATE DUE

2/05 c:/CIRC/DateDue.indd-p.15

A UNIFIED MOMENTUM EQUATION APPROACH FOR FLUID-STRUCTURE INTERACTION (FSI) PROBLEMS WITH STATIONARY BOUNDARIES

By

Jagadish Gattu

A THESIS

Submitted to
Michigan State University
in partial fulfillment of the requirements
for the degree of

MASTER OF SCIENCE

Department of Mechanical Engineering

2005

ABSTRACT

A UNIFIED MOMENTUM EQUATION APPROACH FOR FLUID-STRUCTURE INTERACTION (FSI) PROBLEMS WITH STATIONARY BOUNDARIES

By

Jagadish Gattu

A unified momentum equation approach based on velocity variables is presented for solving fluid-structure interaction problems. This approach has unique advantages in that the momentum equations of the solid and liquid domains are coupled so as to obtain a unified momentum approach allowing to treat the fluid and solid domains as a whole. This is accompanied by a description of spatial discretization over a staggered grid and a fully implicit temporal discretization. The resulting set of nonlinear algebraic equations is solved by using a segregated approach, embedding a SIMPLE algorithm for the pressure calculation. The model has been applied to a test problem of flow between two parallel plates and the numerical results show favorable agreement with those obtained from ABAQUS. Results for other test problems are also presented to demonstrate the capabilities of the present model. Results show that this new method has several advantages over the previous methods such as consistent and uniform discretization, no interfacing algorithms, incorporation of the interface boundary conditions inherently into the formulation while maintaining the system stable by avoiding ill-conditioned systems.

To my family

ACKNOWLEDGMENTS

I would like to express my deepest appreciation to the following people:

To my advisor Dr. Hyungson Ki for his guidance and insight. It has been my pleasure, and indeed privilege to have worked with him. His support, patience and constant encouragement made this work possible. His pure, unselfish and honest passion for the subject will always serve as an example and inspiration for me.

To my committee members Dr. Andre Benard and Dr. Alfred Loos for their valuable time and consideration. Their suggestions and insights helped to further improve this thesis.

To all my friends for the fabulous times, conversations, arguments and ideas.

To my parents (G. Prasada Rao, and G. Bhavani) and sister (G. Tejaswi), for their love and support at all times and showing me the path of honesty and hardwork.

TABLE OF CONTENTS

LI	ST (ST OF FIGURES v		
1	Intr	Introduction		
	1.1	Background and Literature Survey	1	
	1.2	Motivations	7	
	1.3	Summary of the study	8	
2	Equ	nation Formulation	10	
	2.1	Fluid Formulation	10	
	2.2	Solid Formulation	11	
	2.3	Unified Momentum Equation Approach	14	
3	Des	esicretization and Solution Methodology		
	3.1	Spatial Discretization	19	
		3.1.1 Unified Momentum Equation	21	
		3.1.2 Continuity Equation	27	
	3.2	Temporal Discretization	28	
	3.3	Final Equations	29	
	3.4	boundary Conditions	30	

		3.4.1	Liquid domain	30
		3.4.2	Solid domain	31
	3.5	Solution	on Methodology	33
4	Nur	merica	l Tests	38
	4.1	Poiseu	ille flow	39
		4.1.1	Validation	40
		4.1.2	Numerical Results	41
	4.2	Driver	Cavity Problem	51
		4.2.1	Numerical Results	52
5	Cor	nclusio	n	66
6	Fut	ure wo	ork	68
\mathbf{B}_{1}^{2}	BIBLIOGRAPHY			71

LIST OF FIGURES

2.1	Control Volume	16
3.1	Staggered Grid	20
3.2	Nodal arrangement in a Control Volume	22
3.3	Stress on Oblique plane	32
3.4	Flow Chart of the Solution Procedure	37
4.1	Poiseuille flow between parallel plates	39
4.2	Steady state stress distribution in the solid from ABAQUS	42
4.3	Normal stress distribution in x -direction (σ_{xx}) at different time intervals	43
4.4	Normal stress distribution in y -direction (σ_{yy}) at different time intervals	45
4.5	Shear stress distribution (σ_{xy}) at different time intervals	46
4.6	Velocity vector field in the fluid at different time intervals	48
4.7	Velocity vector field in the solid at different time intervals	49
4.8	Stream lines at different time intervals	50
4.9	Schematic of Driven Cavity Flow	51
4.10	Normal stress distribution in x-direction (σ_{xx}) at different time inter-	
	vals	53

4.10	Cont'd	54
4.11	Normal stress distribution in y-direction (σ_{yy}) at different time intervals	56
4.11	Cont'd	57
4.12	Shear stress distribution (σ_{xy}) in the container at different time intervals	58
4.12	Cont'd	59
4.13	Velocity vector field in the fluid at different time intervals	61
4.13	Cont'd	62
4.14	Velocity vector field in the container at different time intervals	63
4.14	Cont'd	64
4 15	Stream lines at different time intervals	65

CHAPTER 1

Introduction

1.1 Background and Literature Survey

A great number of real-life systems, important for industrial applications and academic research, involve interactions amongst a range of physical phenomena (e.g. viscous, turbulent, thermal, chemical, mechanical, electromagnetic or plasma processes). In some systems the time and length scales of processes studied differ in orders of magnitude. Also these interactions can occur between particles of different phases. Fluid-structure interaction is one such important phenomenon, commonly observed in multi-physics problems which is being studied in this thesis. In order to fully realize their potential, and reduce the development time and cost in industries, it is important to understand and thereby develop models with minimum deviation from the real life. Numerical simulations provide an excellent cost effective solution to fully understand and predict the efficiency of a model. Hence this research attempts to develop an effective model with efficient numerical algorithms and

computational techniques to understand and simulate the problems of fluid-structure interaction.

The development of an efficient and accurate solver for fluid-structure problems is still a challenging task in research. In order to solve the problem accurately, both the fluid and structure have to be solved simultaneously. The partitioned method is introduced by Park et al. [29]. In this method, the fluid is solved first and the pressures at the interface are transferred onto the solid domain and then the solid is updated. Once the solid is updated the fluid mesh is updated according to the corresponding deformation in the solid domain and then the cycle repeats. The partitioned approach is preferred because of its ability to use different solvers for fluid and solid domains. This helps in not developing an entirely new method but to use the already existing methods for the fluids and solids. However this method is suitable to problems in which the fluid and the solid are loosely coupled. The main drawbacks of this method are that it has a limited domain of stability [6] and there is always a time lag between the structure and the fluid which can lead to loss of dynamical equivalence between the model and numerical algorithm [4]. Other works trying to improve the stability and the time lag have also been proposed. Introduction of predictor-corrector algorithms and interaction algorithm where the fluid and structure are integrated in time by an explicit fourth order Runge-Kutta scheme [3] are some of the examples which tried to extend the model to strongly coupled problems.

In case of strong interactions, simultaneous solutions or monolithic schemes [6, 3, 17, 25, 19] are preferable in order to get accurate and stable solutions. In monolithic schemes, a single system of equations is developed for the entire region and is solved simultaneously [6] or the system of equations for the fluid and solid are simultaneously solved in a single iteration loop with consistent time integration schemes [3]. If the discretization method is the same for both the solid and liquid, the entire domain is treated as a whole and the convergence of the system is ensured even though the subsystem strongly differs from the whole system. However the monolithic schemes require a common time-step for the entire region which can sometimes reduce the efficiency of the method. Furthermore, the development of single system of equations requires formulation of coupling matrices which are difficult to compute. The final system of equations obtained may also be ill-conditioned in which case appropriate pre-conditioners [17] are required. Comparisons were made between the monolithic and partitioned approaches [25] to get a better understanding of them.

Coming to the discretization techniques, a wide range of techniques are available in the literature. A Lagrangian formulation [23] has the advantage of clear marking and tracking of the boundaries and is more suited to solids since the boundaries deform with the solid. When the fluid is modeled using Lagrangian approach the mesh deformation in the fluid region becomes unmanageable and so mesh regeneration is often sought which is computationally expensive and is avoided as much as possible. On the other hand an Eulerian [30, 31] approach has the clear advantage that strong deformations can be taken care of but it comes at an

expense of precise interface definition. Due to these restrictions, an intermediate method known as Arbitrary Lagrangian-Eulerian method [18, 12], which combines the advantages of the two methods was developed. The generalized descriptions for ALE formulations were initially developed for finite difference formulations [18]. Later, Donea et al. [12] first applied ALE concepts to finite element methods to solve transient dynamic fluid-structure interaction problems.

The main advantage of ALE is the ability to move the fluid mesh independent of the motion of the fluid itself. This allows the fluid nodes to remain fixed with the solid nodes and hence the fluid-structure coupling is simplified. The advantages in ALE come with a price. The freedom in moving the fluid mesh offered by the ALE can be overshadowed by the burden of specifying grid velocities. Also, even though the ALE formulation overcomes the problem of boundary clarity, it still has the problem of handling large deformations. Although most of the ALE formulations have mesh updating, when the distortions become large, mesh regeneration becomes unavoidable. Researchers [32] tried to develop possible ways to control the distortion of the mesh. Later more features of the fluid modeling like turbulence have been incorporated into the ALE model [36, 2]. Despite the relative advantages of ALE, the requirement of re-meshing at some point introduces artificial diffusivity, and is also difficult and time-consuming to perform with sufficient robustness and accuracy for three dimensional problems. Due to this reason researchers developed other numerical methods like Fictitious Domain [1, 11, 5, 14], space-time elements[19, 16, 7, 20, 21, 15, 34].

Fictitious domain methods are advantageous for the fact that that they allow the use of fairly structured meshes on a simple shape auxiliary domain containing the actual one, allowing fast solvers. Glowinski et al. [14] proposed a model taking the systematic advantage of the Lagrange multipliers associated with the boundary condition imposed on the actual boundary. Later Baijens [1] developed a method combining the fictitious domain method and the mortar element method for solving fluid-structure interaction problems. However, these methods are accompanied by the need to store information concerning the actual geometry which is not trivial for complex geometries.

In elastodynamics, time-discontinuous stabilized space-time elements were introduced by Hughes and Hulbert [20]. Brooks and Hughes [7] and Hughes et al. [21] presented stabilized finite elements, while Tezduyar et al. [34] and Hansbo [15] applied the space-time formulation for solving the incompressible Navier-Stokes equations on moving meshes. Later these were extended to solve fluid-structure interaction problems. Hubner et al. [19] proposed a monolithic approach based on velocity variables for both solid and liquid domains, while Hansbo et al. [16] combined Nitsche's method with space-time finite elements to mimic ALE simulations. The advantage of this method is its consistent discretization of both space and time domain including space-time adaptive meshes. Furthermore the movement of the fluid domain is natural as the elements vary with time. However the main drawback is the limitation of finite elements in time.

On the other hand, a family of methods called meshless methods has been developed. These ideas were proposed by Nayroles et al. [26], later used by Idelsohn et al. [23]. The advantages are high order continuity at element boundaries and easy generation of adequate discretization meshes for complex tri-dimensional domains. Nevertheless they follow the Lagrangian approach and face difficulties with large deformations.

The other important discretization technique for doing numerical simulation is finite volume method (FVM) which is more used for solving fluid problems. Eventhough finite element and finite volume methods share a number of features like mesh discretization and approximation, they take a very different approach in treating the convective terms. For solving Navier-Stokes equations the FVM is more consistent and hence preferable over the FEM [22]. Due to this reason researchers [30, 31] have developed finite volume methods to solve fluid-structure interaction. Slone et al. [30] developed a finite volume method for solving dynamic structural problems and later Slone et al. [31] applied it to solve dynamic fluid-structure interaction problems.

Another important concern in discretization is transfer of information from one domain to the other. The role of fluid structure interfacing (FSI) algorithms is to ensure appropriate coupling between the solid and liquid domains along their interface. The types of interfaces can be classified as conforming and non-conforming meshes. Examples of FSI algorithms for conforming meshes include fluid structure

interaction of the ALE (permanent) type (FSA) [8] and Uniform Pressure (UP) [9] methods. In conforming interfaces the fluid and structure elements must have the same size at the interface. This has a major disadvantage in that the degree of resolution required for liquid and solid is different and having same sized elements at the interface compromises either the solid or the liquid resolution for the other. These disadvantages have led the path to FSI algorithms [10, 13] for non-conforming meshes which is more general and is more suitable to partitioned methods which are preferred due to their ability to use established solution methods in each discipline.

1.2 Motivations

In summary, the various approaches used in the past to tackle FSI problems can be generally classified in terms of numerical methods (Monolithic and Partitioned), grid generation and discretization techniques (Lagrangian, Eulerian, ALE, Fictious domain methods, Space-time and meshless methods) and interfacing algorithms (FSA and UP based on conforming and non-conforming meshes). These different approaches try to reduce the differences in the formulation of fluid and solid domains which can be generalized as following; requirements in terms of mesh reference, grid resolution and variables to be solved for solid and liquid domains. These differences end up as extra costs in terms of coupling two systems of equations, providing interface algorithms to transfer data from one domain to other, and mesh movement. An ideal method to solve the fluid-structure interaction problem would be one which has a uniform and consistent spatial and temporal discretization along with a mechanism

to interact among the phases freely without any interfacing algorithms. Some of the attempts to reduce these differences are displacement based elements for fluids [35], potential based formulation for fluids [28, 27, 24, 33] and velocity based formulations for solids [19]. However they only succeeded partially in improving the solution. The aim of this research is to further move a step closer to reducing the differences between the fluid and solid formulations and come with an approach which can interact freely among the phases without any need for interfacing algorithms along with a consistent discretization throughout the domain.

1.3 Summary of the Study

In this research a novel monolithic finite volume scheme based on a unified momentum equation with velocity variables is proposed. This approach has been tested and validated by applying it to a Poiseuille flow between parallel plates. The numerical results of the flow and stress fields are in good agreement with those obtained from analytical computation. Later this method is successfully applied to a driven cavity problem. The results from the simulations show that this approach has several unique advantages. Firstly, the momentum equations of the solid and liquid domains are coupled to obtain a unified momentum approach. This allows in treating the fluid and solid domains as a whole which means that a single numerical algorithm can be applied to both phases. Also the interface boundary conditions, such as continuity of velocities and displacements, and consideration of shear and normal stresses, have been automatically taken into account during the formulation. This

means that there is no need to match the boundary conditions with this method. Computationally, the consideration of velocity variables for the solid domain removes the burden of interpolation of variables from one domain to other. On the other hand the finite volume method makes it simple to understand and easy to extend the method to more complicated and unstructured problems. Also this method does not generate ill-conditioned matrices unlike other monolithic schemes.

The organization of the thesis is as follows. In Chapter 2, we describe the governing equations for fluid and solid domains and construct the unified momentum equation governing the fluid-structure problem. Chapter 3 deals with the discretization and solution methodology used to implement the unified momentum equation approach. Chapter 4 consists of test problems which are solved using the current approach along with the detailed discussion of the results. Conclusions are made in Chapter 5 while Chapter 6 consists of future work.

CHAPTER 2

Equation Formulation

In this section the problem is formulated and the necessary assumptions are specified.

The fluid is considered as newtonian while the solid is modeled using elastodynamic model. These are further explained in the coming sections.

2.1 Fluid Formulation

The governing equations for the fluid flow consist primarily of the Navier Stoke's equation, including conservation of mass and momentum. The conservation of mass is represented by the continuity equation (Equation 2.1) which is required to close the set of equations.

• Continuity Equation

$$\frac{\partial \rho}{\partial t} + \nabla \cdot (\rho \mathbf{u}) = 0 \tag{2.1}$$

• Conservation of Momentum

$$\frac{D(\rho \mathbf{u})}{Dt} = \nabla \cdot \boldsymbol{\sigma}_f + \mathbf{f} \tag{2.2}$$

where σ_f is the stress vector, **f** is the external force,

$$\boldsymbol{\sigma}_f = -p\mathbf{I} + 2\mu \boldsymbol{R} \tag{2.3}$$

where μ denotes viscous constant and R is the rate of strain,

$$\mathbf{R} = \frac{1}{2} (\nabla \mathbf{u} + \nabla \mathbf{u}^T) \tag{2.4}$$

where **u** represents the velocity vector. Substituting Equations 2.3 and 2.4 in Equation 2.2 and rearranging the terms we have

$$\frac{\partial(\rho\mathbf{u})}{\partial t} + \nabla \cdot (\rho\mathbf{u}\mathbf{u} + \mu\nabla\mathbf{u} - p\mathbf{I}) = \mathbf{f}$$
 (2.5)

In the above Equation 2.5 the term $\nabla \cdot (\rho \mathbf{u} \mathbf{u})$ represents the convective terms whereas $\mu \nabla \mathbf{u}$ represents the viscous terms.

2.2 Solid Formulation

The solid domain is formulated using elastodynamic equation representing the conservation of momentum. For the case of solids, the continuity equation is not required as it is used to determine the density, which for the case of solids is assumed to be constant. Hence the elastodynamic equation is sufficient to solve for the displacement or velocity variables.

• Conservation of Momentum (elastodynamic Equation)

$$\rho \frac{\partial^2 \mathbf{d}}{\partial t^2} = \nabla \cdot \boldsymbol{\sigma}_s + \mathbf{f} \tag{2.6}$$

Here, **d** is displacement vector defined as

$$\mathbf{d} = d_x \hat{i} + d_y \hat{j} + d_z \hat{k} \tag{2.7}$$

and σ_s is the stress temsor for solids, and \mathbf{f} is the external body force that includes gravity, electromagnetic forces, and phase transformation terms. If the left-hand side of Equation 2.6 is written in terms of velocity \mathbf{u} and convective terms included, the following momentum equation is obtained.

$$\frac{D(\rho \mathbf{u})}{Dt} = \nabla \cdot \boldsymbol{\sigma}_s + \mathbf{f} \tag{2.8}$$

Here, the stress vector is defined as,

$$\sigma_s = 2\tilde{\mu}\varepsilon + (\tilde{\lambda}\mathrm{Tr}(\varepsilon))\mathrm{I} \tag{2.9}$$

where ε represents the strain tensor,

$$\boldsymbol{\varepsilon} = \frac{1}{2} (\nabla \mathbf{d} + \nabla \mathbf{d}^T) \tag{2.10}$$

and $\tilde{\lambda}$ and $\tilde{\mu}$ are Lame's constants, defined in terms of modulus of elasticity (E) and Poisson's ratio (ν).

$$\tilde{\lambda} = \frac{E\nu}{(1+\nu)(1-2\nu)} \quad \text{and} \quad \tilde{\mu} = \frac{E}{2(1+\nu)}$$
 (2.11)

Substituting Equation 2.10 into Equation 2.9 and rearranging terms the following equation for the stress tensor is obtained.

$$\sigma_s = \tilde{\mu}(\nabla \mathbf{d}) + (\tilde{\lambda} + \tilde{\mu})(\nabla \cdot \mathbf{d})\mathbf{I}$$
(2.12)

Substituting the Equation 2.12 in Equation 2.8 and expanding the total derivative, we obtain

$$\frac{\partial(\rho\mathbf{u})}{\partial t} + \nabla \cdot (\rho\mathbf{u}\mathbf{u}) = \nabla \cdot \left(\tilde{\mu}(\nabla\mathbf{d}) + (\tilde{\lambda} + \tilde{\mu})(\nabla \cdot \mathbf{d})\mathbf{I}\right) + \mathbf{f}$$
(2.13)

Finally, rearranging the Equation 2.13, we obtain the following form of the momentum equation for solids.

$$\frac{\partial(\rho\mathbf{u})}{\partial t} + \nabla \cdot \left(\rho\mathbf{u}\mathbf{u} - \tilde{\mu}(\nabla\mathbf{d}) - (\tilde{\lambda} + \tilde{\mu})(\nabla \cdot \mathbf{d})\mathbf{I}\right) = \mathbf{f}$$
 (2.14)

The term ρ uu in the Equation 2.14 represents the convective terms. Unlike the case for fluids, the displacements and velocities in the solid domain are so small that these convective terms can be neglected. Some of the evident and direct differences between the fluid and solid formulations which can be noticed in the above formulations are the requirement of the continuity equation and the convective terms in the fluid domain. For the fluid, the convective terms contribute significant amount of flux, where as the continuity equation is required to close the set of equations. This is however not the case with solids. The next section focusses on reducing these differences and representing them as the unified momentum equation common to both the domains.

2.3 Unified Momentum Equation Approach

The unified momentum equation enables us to combine both the momentum equations into a single generalized equation which is then solved for the entire domain. By observing the Equations 2.5 and 2.14, the unified momentum equation can be derived as

$$\rho \frac{\partial \mathbf{u}}{\partial t} + \nabla \cdot \mathbf{J} = \mathbf{f} \tag{2.15}$$

where J represents the stress tensor given as

$$\mathbf{J} = \begin{cases} \mathbf{J}_f = \rho \mathbf{u} \mathbf{u} - \mu \nabla \mathbf{u} + p \mathbf{I} & \text{for fluids} \\ \mathbf{J}_s = \rho \mathbf{u} \mathbf{u} - \tilde{\mu} (\nabla \mathbf{d}) - (\tilde{\lambda} + \tilde{\mu}) (\nabla \cdot \mathbf{d}) \mathbf{I} & \text{for solids} \end{cases}$$
(2.16)

The stress tensor J is different from the actual stress tensor σ in that it includes the convective stress ρuu . Observe that J_f and J_s are very similar.

It is important to note that the unified momentum equation is not just a way of representation, it symbolizes the Newton's second Law of motion and every term in Equation 2.15 has its own physical meaning. The term J has the units of stress equivalent to force acting per unit area and J is calculated based on the type of phase. So, this principle can further be extended to other phases provided J can be explicitly represented as a function of variables pertaining to that phase. This is the first step in moving towards developing a single numerical algorithm which can be applied to both phases.

Even though there are several numerical methods to solve the conservation

equations, the finite volume method is particularly suitable for the unified momentum equation formulation. The finite volume method starts with the integral form of the conservation equation to obtain a final equation with flux contributions from each side of the control volume. The Navier-Stokes equations have the property that the momentum in any control volume (microscopic or macroscopic) is changed only by flow through the surface, forces acting on the surface, and volumetric body forces. This important property is inherited by the discretized equation if the Finite Volume approach is used and surface fluxes for adjacent control volumes are identical. If this is done, then the integral over the entire domain, being the sum of the integrals over the microscopic control volumes, reduces to a sum over the surface of the domain. Overall mass conservation follows in the same way from the continuity equation. This method is particularly suitable for the unified momentum equation approach as the flux contributions from each side of the control volume have already been defined in the unified momentum equation. This is another important advantage with the unified momentum equation approach. This advantage becomes more evident as we proceed further through this section. Writing the Equation 2.15 using indicial notation, we have

$$\frac{\partial(\rho u)}{\partial t} + \frac{\partial J_{ij}}{\partial x_i} = f_i \tag{2.17}$$

As an example, let's consider the x-component of the unified momentum equation

$$\frac{\partial(\rho u)}{\partial t} + \frac{\partial J_{xx}}{\partial x} + \frac{\partial J_{xy}}{\partial y} + \frac{\partial J_{xz}}{\partial z} = f_x \tag{2.18}$$

Integrating Equation 2.18 over a control volume of dimensions $\triangle x$, $\triangle y$ and $\triangle z$ we obtain

$$\oint_{\triangle V} \left(\frac{\partial (\rho u)}{\partial t} + \frac{\partial J_{xx}}{\partial x} + \frac{\partial J_{xy}}{\partial y} + \frac{\partial J_{xz}}{\partial z} \right) = \oint_{\triangle V} f_x \tag{2.19}$$

which upon expansion results in

$$\frac{\partial (\tilde{\rho}u)}{\partial t} \Delta x \Delta y \Delta z + \left((J_{xx})_e - (J_{xx})_w \right) \Delta y \Delta z + \left((J_{xy})_t - (J_{xy})_b \right) \Delta x \Delta z + \left((J_{xz})_n - (J_{xz})_s \right) \Delta x \Delta y = \bar{f}_x \Delta x \Delta y \Delta z$$

or

$$\frac{\partial(\tilde{\rho}u)}{\partial t}\Delta V + \left((J_{xx})_e - (J_{xx})_w\right)\Delta A_x + \left((J_{xy})_t - (J_{xy})_b\right)\Delta A_y + \left((J_{xz})_n - (J_{xz})_s\right)\Delta A_z = \bar{f}_x\Delta V \quad (2.20)$$

Here, we define the volume of cell and the three cell face areas in x-, y-,

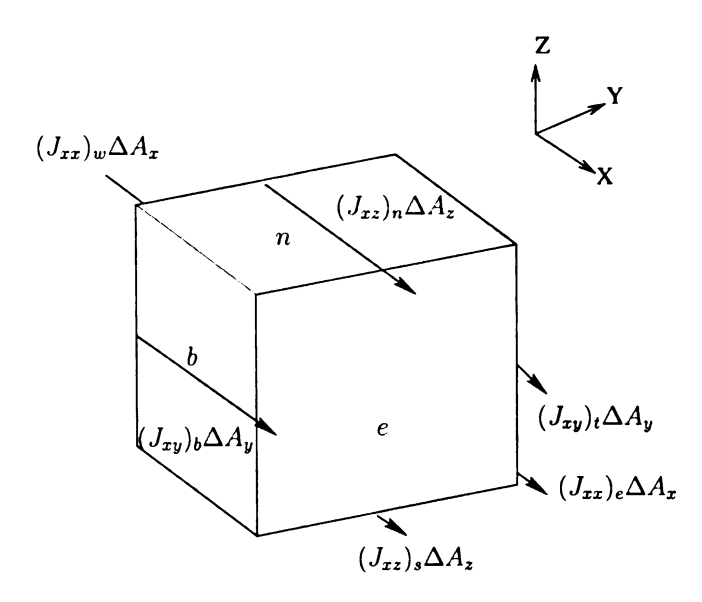


Figure 2.1. Control volume

z-directions as $\Delta V,~\Delta A_x,~\Delta A_y$ and ΔA_z respectively (Figure 2.1). Also $\bar{\rho}$ is the

volume-averaged density, and \bar{f}_x is the volume-averaged body force. The subscripts e, w, t, b, n and s denote east (+x), west (-x), top (+y), bottom (-y), north (+z), and south (-z) faces o the cell (Figure 2.1). For example, $(J_{xx})_e$ denotes the normal stress in the x-direction at the cell face e, and $(J_{xy})_t$ is the shear stress at the cell face t. Since, J has the units of stress, the terms containing J in the Equation 2.20. Therefore, the physical meaning of the term $(J_{xz})_n \Delta A_z$ is the surface force acting on the surface n in the x-direction.

A careful observation of the Equation 2.20 emphasizes that it can be applied to any control volume independent of whether the control volume is surrounded by fluid or solid or both. When a face is surrounded by a fluid, the stress J at that face can be evaluated using J_f given by the Equation 2.16. Alternately, When the face is surrounded by solid, the stress J can be evaluated using J_s given by the Equation 2.16. This allows us to solve for the momentum equation for the entire domain using a single algorithm without having to solve for fluid and solid domains separately.

As an example, consider the surfaces e, b, n are surrounded by a solid and the rest of the surfaces are surrounded by a fluid, then J_s is used to evaluate $(J_{xx})_e$, $(J_{xy})_b$, $(J_{xz})_n$ and J_f is used to evaluate $(J_{xx})_w$, $(J_{xy})_t$ and $(J_{xz})_s$. In this case we

obtain the following momentum equation for the cell

$$\frac{\partial(\bar{\rho}u)}{\partial t}\Delta V + \left(\rho u u - \bar{\mu}\frac{\partial d_x}{\partial x} - (\tilde{\lambda} + \tilde{\mu})\left(\frac{\partial d_x}{\partial t} + \frac{\partial d_y}{\partial t} + \frac{\partial d_z}{\partial t}\right)\right)_e \Delta A_x - \left(\rho u u - \mu \frac{\partial u}{\partial x} + p\right)_w \Delta A_x + \left(\rho v u - \mu \frac{\partial u}{\partial y}\right)_t \Delta A_y - \left(\tilde{\mu}\left(\frac{\partial d_x}{\partial y} + \frac{\partial d_y}{\partial x}\right)\right)_b \Delta A_y - \left(\tilde{\mu}\left(\frac{\partial d_z}{\partial x} + \frac{\partial d_z}{\partial z}\right)\right)_n \Delta A_z - \left(\rho w u - \mu \frac{\partial u}{\partial z}\right)_s \Delta A_z = \bar{f}_x \Delta V \quad (2.21)$$

In this way it is possible to tailor the momentum to any kind of fluid-structure interface configurations. Next, discretization of the governing equations is discussed in Chapter 3.

CHAPTER 3

Desicretization and Solution

Methodology

In this section, the spatial and temporal discretization of the conservation equations is discussed in detail. First, the spatial discretization is discussed which is then followed by temporal discretization. Next, the boundary conditions are presented for both the fluid and solid domain. Finally, the solution methodology will be discussed in detail.

3.1 Spatial Discretization

A staggered grid is considered for the spatial discretization. In Cartesian coordinates, the staggered arrangement introduced by Harlow and Welsh (1965) offers several advantages over the collocated arrangement. This arrangement for a two-dimensional grid is shown in Figure 3.1. A dot indicates the position where a scalar quantity such as pressure is stored, while the arrows indicate the points where velocity components

are stored whose direction is represented by the arrow direction. The shaded and non-shaded regions indicate the different phases solid and fluid respectively. For a three dimensional case, a staggered grid will have 4 different control volumes corresponding to three velocity components and a scalar variable.

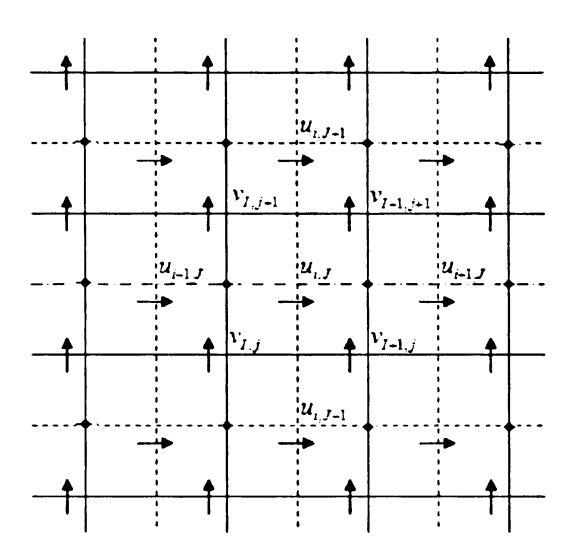


Figure 3.1. Staggered grid

Despite the increased number of control volumes the staggered grid is preferred due to its advantages. The advantages being pressure and diffusion terms can be naturally approximated by central difference approximations without interpolation, the velocity derivatives needed for the diffusive terms can be readily computed at the CV faces and the evaluation of mass fluxes in the continuity equation on the faces of a pressure CV is straightforward. But the biggest advantage of the staggered grid is the strong coupling between the velocities and the pressure. These positive features of the staggered grid justify the selection of staggered grid over the collocated grid as it also avoids some types of convergence problems and oscillation in pressure and

velocity fields.

3.1.1 Unified Momentum Equation

The discretization of the unified momentum equation is done at two levels. The first level is the discretization of the unified momentum equation into flux terms over a single control volume. Next, the resulting equation with flux terms is further discretized in terms of the grid variables in the second level. The flux terms obtained from the first level of discretization include both J_f and J_s which has been discussed in Section 2.3. Each of these terms is then separately discretized to complete the discretization process. The generalized equation obtained by integrating the unified momentum equation over a control volume can be defined as

$$\frac{\partial (\tilde{\rho}u_i)}{\partial t} \Delta V + \left((J_{ij})_{j^+} - (J_{ij})_{j^-} \right) \Delta A_i = \bar{f}_i \Delta V \tag{3.1}$$

The term $(J_{ij})_{j+}$ represents the ij^{th} component of the J stress tensor, whereas the subscript j^+ indicates the face in the positive direction of the j-axis in the control volume at which the flux is being evaluated. Hence for a 3-dimensional control volume we have three different fluxes, each of which needs to be evaluated at two different faces and hence totally 6 fluxes show up in Equation 3.1. This completes the first level of discretization.

The Equation 3.1 consists of the flux terms which are further to be discretized in order to write the conservation equations in terms of the variables, which are being solved for. The flux term is discretized for different cases corresponding to the region in which the face is located. These cases of discretization are further explained in the coming sections. Before continuing further, the notation followed

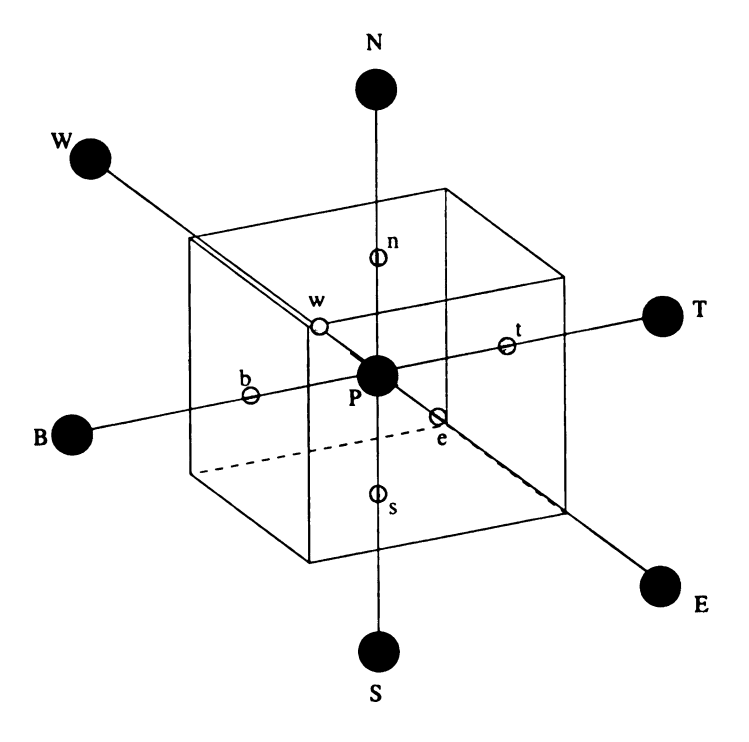


Figure 3.2. Nodal arrangement in a control volume

in the discretization needs to be addressed. All the variables are represented with respect to the cell center. For a given control volume shown in Figure 3.2, the node P represents the cell center whereas the nodes E, W, N, S, T and B represent the cell centers of its neighboring cells. Also, the face centers are represented by small letters e, w, n, s, t and b corresponding to their directions.

Fluid Face

In this case the face completely lies in the fluid region. Hence the flux terms can be evaluated using the J_f obtained from the Equation 2.16. Consider a component J_{ij} ,

which needs to be evaluated at j^+ face or j^- face. Now it can be written as

$$J_{ij} = \rho u_i u_j - \mu \frac{\partial u_j}{\partial x_j} + p \delta_{ij}$$
 (3.2)

The discretized representation of the flux term is given for all the three u, v and w control volumes. For each control volume, six flux terms need to be evaluated which are provided below. \bar{J} indicates the stress J_{ij} multiplied with the area of the face $A_{j\pm}$ at which it is being evaluated.

• u-control volume

$$\bar{J}_e^u = a_E(u_E - u_P) + p_e$$
 $\bar{J}_w^u = a_W(u_P - u_W) - p_w$
 $\bar{J}_n^u = a_N(u_N - u_P)$ $\bar{J}_s^u = a_S(u_P - u_S)$
 $\bar{J}_t^u = a_T(u_T - u_P)$ $\bar{J}_b^u = a_B(u_P - u_B)$

• v-control volume

$$ar{J}_e^v = a_E(v_E - v_P)$$
 $ar{J}_w^v = a_W(v_P - v_W)$ $ar{J}_n^v = a_N(v_N - v_P)$ $ar{J}_s^v = a_S(v_P - v_S)$ $ar{J}_t^v = a_T(v_T - v_P) + p_t$ $ar{J}_b^v = a_B(v_P - v_B) - p_b$

w-control volume

$$ar{J}_{e}^{w} = a_{E}(w_{E} - w_{P})$$
 $ar{J}_{w}^{w} = a_{W}(w_{P} - w_{W})$ $ar{J}_{n}^{w} = a_{N}(w_{N} - w_{P}) + p_{n}$ $ar{J}_{s}^{w} = a_{S}(w_{P} - w_{S}) - p_{s}$ $ar{J}_{t}^{w} = a_{T}(w_{T} - w_{P})$ $ar{J}_{b}^{w} = a_{B}(w_{P} - w_{B})$

where

$$a_E = D_e + \max(-F_e, 0)$$
 $a_W = D_w + \max(F_w, 0)$
 $a_N = D_n + \max(-F_n, 0)$ $a_S = D_s + \max(F_s, 0)$
 $a_T = D_t + \max(-F_t, 0)$ $a_B = D_b + \max(F_b, 0)$

where F is the mass flux arising due to the convection terms and D is the diffusion flux or conductance arising due to the diffusion terms. These are defined as follows.

$$F_{e} = (\rho u)_{e} \Delta y \Delta z \qquad F_{w} = (\rho u)_{w} \Delta y \Delta z$$

$$F_{n} = (\rho w)_{n} \Delta z \Delta x \qquad F_{s} = (\rho w)_{s} \Delta z \Delta x$$

$$F_{t} = (\rho v)_{t} \Delta x \Delta y \qquad F_{b} = (\rho v)_{b} \Delta x \Delta y$$

$$D_{e} = \frac{\mu_{e} \Delta y \Delta z}{(\delta x)_{e}} \qquad D_{w} = \frac{\mu_{w} \Delta y \Delta z}{(\delta x)_{w}}$$

$$D_{n} = \frac{\mu_{n} \Delta z \Delta x}{(\delta y)_{n}} \qquad D_{s} = \frac{\mu_{s} \Delta z \Delta x}{(\delta y)_{s}}$$

$$D_{t} = \frac{\mu_{t} \Delta x \Delta y}{(\delta z)_{t}} \qquad D_{b} = \frac{\mu_{b} \Delta x \Delta y}{(\delta z)_{b}}$$

Solid Face

In this case, the face completely lies entirely in the solid domain. Hence the flux can be calculated from the Equation 2.16. The discretized representation of the flux terms is given in sync with the notation in Figure 3.2. As discussed earlier, for each control volume, six flux terms need to be evaluated which are provided below. \bar{J} indicates the stress J_{ij} multiplied with the area of the face $A_{j\pm}$ at which it is being evaluated.

• u-control volume

$$\bar{J}_{e}^{u} = \frac{(\tilde{\mu} + \tilde{\lambda})A_{e}}{\Delta x} (d_{x,E} - d_{x,P}) + \tilde{\lambda}A_{e} (\frac{d_{y,te} - d_{y,be}}{\Delta y} + \frac{d_{z,ne} - d_{z,se}}{\Delta z})$$

$$\bar{J}_{w}^{u} = \frac{(\tilde{\mu} + \tilde{\lambda})A_{w}}{\Delta x} (d_{x,P} - d_{x,W}) + \tilde{\lambda}A_{w} (\frac{d_{y,tw} - d_{y,bw}}{\Delta y} + \frac{d_{z,nw} - d_{z,sw}}{\Delta z})$$

$$\bar{J}_{t}^{u} = \tilde{\mu}A_{t} (\frac{d_{x,T} - d_{x,P}}{\Delta y} + \frac{d_{y,te} - d_{y,tw}}{\Delta x})$$

$$\bar{J}_{b}^{u} = \tilde{\mu}A_{b} (\frac{d_{x,P} - d_{x,B}}{\Delta y} + \frac{d_{y,be} - d_{y,bw}}{\Delta x})$$

$$\bar{J}_{n}^{u} = \tilde{\mu}A_{n} (\frac{d_{x,N} - d_{x,P}}{\Delta z} + \frac{d_{z,ne} - d_{z,nw}}{\Delta x})$$

$$\bar{J}_{s}^{u} = \tilde{\mu}A_{s} (\frac{d_{x,P} - d_{x,S}}{\Delta z} + \frac{d_{z,se} - d_{z,sw}}{\Delta x})$$

• v-control volume

$$\begin{split} \bar{J}_{t}^{v} &= \frac{(\tilde{\mu} + \tilde{\lambda})A_{t}}{\Delta y}(d_{y,T} - d_{y,P}) + \tilde{\lambda}A_{t}(\frac{d_{x,te} - d_{x,tw}}{\Delta x} + \frac{d_{z,tn} - d_{z,ts}}{\Delta z}) \\ \bar{J}_{b}^{v} &= \frac{(\tilde{\mu} + \tilde{\lambda})A_{b}}{\Delta y}(d_{x,P} - d_{x,B}) + \tilde{\lambda}A_{b}(\frac{d_{x,be} - d_{x,bw}}{\Delta x} + \frac{d_{z,bn} - d_{z,bs}}{\Delta z}) \\ \bar{J}_{e}^{v} &= \tilde{\mu}A_{e}(\frac{d_{y,E} - d_{y,P}}{\Delta x} + \frac{d_{x,et} - d_{y,eb}}{\Delta y}) \\ \bar{J}_{w}^{v} &= \tilde{\mu}A_{w}(\frac{d_{y,P} - d_{y,W}}{\Delta x} + \frac{d_{x,wt} - d_{x,wb}}{\Delta y}) \\ \bar{J}_{n}^{v} &= \tilde{\mu}A_{n}(\frac{d_{y,N} - d_{y,P}}{\Delta z} + \frac{d_{z,nt} - d_{z,nb}}{\Delta y}) \\ \bar{J}_{s}^{v} &= \tilde{\mu}A_{s}(\frac{d_{y,P} - d_{y,S}}{\Delta z} + \frac{d_{z,st} - d_{z,sb}}{\Delta y}) \end{split}$$

w-control volume

$$\bar{J}_{n}^{w} = \frac{(\tilde{\mu} + \tilde{\lambda})A_{n}}{\Delta z}(d_{z,N} - d_{z,P}) + \tilde{\lambda}A_{n}(\frac{d_{x,ne} - d_{x,nw}}{\Delta x} + \frac{d_{y,nt} - d_{y,nb}}{\Delta y})$$

$$\bar{J}_{s}^{w} = \frac{(\tilde{\mu} + \tilde{\lambda})A_{s}}{\Delta z}(d_{z,P} - d_{z,S}) + \tilde{\lambda}A_{s}(\frac{d_{x,se} - d_{x,sw}}{\Delta x} + \frac{d_{y,st} - d_{y,sb}}{\Delta y})$$

$$\bar{J}_{e}^{w} = \tilde{\mu}A_{e}(\frac{d_{z,E} - d_{z,P}}{\Delta x} + \frac{d_{x,en} - d_{x,es}}{\Delta z})$$

$$\bar{J}_{w}^{w} = \tilde{\mu}A_{w}(\frac{d_{z,P} - d_{z,W}}{\Delta x} + \frac{d_{x,wn} - d_{x,ws}}{\Delta z})$$

$$\bar{J}_{t}^{w} = \tilde{\mu}A_{t}(\frac{d_{z,T} - d_{z,P}}{\Delta y} + \frac{d_{y,tn} - d_{y,es}}{\Delta z})$$

$$\bar{J}_{b}^{w} = \tilde{\mu}A_{b}(\frac{d_{z,P} - d_{z,B}}{\Delta y} + \frac{d_{y,bn} - d_{y,bs}}{\Delta z})$$

where $d_{i,mn}$ indicates the *i* component of displacement vector and the subscript mn indicates the position of the displacement component d_i . mn indicates the center of the edge at the intersection of m and n faces. For example, the subscript x, es indicates the x-component of the displacement vector at the center of edge at the intersection of east and south faces.

As observed from the discretized equations for the solid and liquid faces, one major difference can be noticed. The interdependence of individual momentum components in solid stress is much higher than in the case of liquid. This is due to the influence of y and z components on fluxes for the u-control volume and similarly the influence of other components in evaluating flux terms for the solid face for v and v control volumes. This is much less in the case of flux terms for liquid face.

3.1.2 Continuity Equation

As mentioned earlier, the continuity equation (Equation 2.1) appears because of the liquid domain. The unified momentum equation consists of pressure terms coming from the flux terms pertaining to the fluid domain. Since pressure is also an unknown variable which needs to be solved for, the continuity equation is required to close the set of equations. However the numerical algorithm will take care of the continuity equation in such a way, that no special consideration is required because of this difference between the two phases. This will addressed in the solution section.

The velocity field in the liquid domain is subject to the constraint that it should satisfy continuity equation. Hence substituting the velocities obtained from momentum equations with an incorrect or guessed pressure field in the continuity equation and rearranging the terms, one can rewrite the continuity equation in terms of the velocities and pressures. Following this basic principle, the pressure correction equation based on SIMPLE algorithm can be written as

$$a_{P}^{p}p_{P}^{'} = a_{E}^{p}p_{E}^{'} + a_{W}^{p}p_{W}^{'} + a_{N}^{p}p_{N}^{'} + a_{S}^{p}p_{S}^{'} + a_{T}^{p}p_{T}^{'} + a_{B}^{p}p_{B}^{'} + S_{P}^{'}$$

$$(3.6)$$

where

$$a_E^p = (\rho dA)_e \qquad a_W^p = (\rho dA)_w$$

$$a_N^p = (\rho dA)_n \qquad a_S^p = (\rho dA)_s \qquad (3.7)$$

$$a_T^p = (\rho dA)_t \qquad a_R^p = (\rho dA)_b$$

$$a_P^p = a_E^p + a_W^p + a_N^p + a_S^p + a_T^p + a_B^p (3.8)$$

and

$$d = \frac{A}{a_P} \tag{3.9}$$

where A represents the area of the face at which d is being evaluated and a_P is given by the discretized momentum equation corresponding to the variable at the face center. For example if the face center consists the x-component of the velocity vector, a_P corresponds to the coefficient from the discretized u-momentum equation.

Equation 3.6 represents the discretised continuity equation as an equation for pressure correction p'. The source term S' in the equation is the continuity imbalance arising from the incorrect velocity field.

3.2 Temporal Discretization

The present algorithm employs a fully implicit scheme for temporal discretization for all variables. Considering a function ϕ which is dependent on variables u_l . Following the implicit scheme we have

$$\frac{du_i}{dt} = \phi(u_l)$$

$$\implies u_i^{n+1} = u_i^n + \phi(u_l)^{n+1} \Delta t$$
(3.10)

Hence from Equation 3.10 it can be noticed unknown quantities appear on both sides of the equation and hence need a set of equations which have to be solved

simultaneously to determine the unknown variables.

The principal reason for using implicit solution methods, which are more complex to implement and require more computational effort in each solution step, is due to the fact that it is unconditionally stable, allowing for large time-step sizes. However since the unified momentum equations for each component and the continuity equation are being solved solved in a staggered manner, it is not reasonable to assume a very large time step to get reasonably accurate results. Another important advantage of the implicit method is its ability to obtain accurate intermediate results. Even though time marching explicit schemes are computationally efficient than the implicit schemes, they can only be used to obtain the steady state solution.

3.3 Final Equations

As mentioned above, the discretized equations are written in terms of the field variables i.e., velocities in the fluid region and displacements in the solid region. In order to avoid the interpolation of variables from one domain to another which is one of the disadvantages of the earlier methods, the displacements in the solid domain from the flux terms are converted to velocities. The following first order implicit formulation is used to represent the equations in terms of velocities throughout the domain.

$$d^{n+1} = \int_{t(n)}^{t(n+1)} u \ dt + d^n \approx u^{n+1} \Delta t + d^n$$
 (3.11)

Since the displacements at the n^{th} level are known the last term in Equation 3.11 is a known quantity and hence goes to the source term in the final discretized equation with velocities throughout the domain. Finally, rearranging the discretized equations, they can be represented as

$$a_P \ u_P^{n+1} = \Sigma_{nb} \ a_{nb} \ u_{nb}^{n+1} + S_u \tag{3.12}$$

where P is the index of an arbitrary velocity node representing the center of the control volume, and index nb denotes neighbor points corresponding to the centers of the neighboring cells, that appear in the discretized momentum equation. The source term S contains all of the terms that may be explicitly computed in terms of u^n as well as any body force or other linearized terms that may depend on u^n .

3.4 Boundary Conditions

3.4.1 Liquid domain

Usually there are three types of boundary conditions which are common for the liquid domain and they are inlet, outlet and wall boundary conditions. These are discussed further in this section.

• Inlet

At an inlet boundary, all quantities have to be prescribed or be able to calculate from the known variable values at the inlet boundary.

• Outlet

At the outlet, most of the quantities are extrapolated along grid lines from the interior to the boundary. The simplest approximation of zero gradient along grid lines is followed in this present work.

• Wall

A no-slip condition is applied at the wall boundary. This condition follows from the fact that viscous fluids stick to solid boundary without any slip. Hence, the following condition is applied at the wall

$$u = u_{wall} \tag{3.13}$$

The above mentioned boundary conditions can be applied in two different ways. The first one is to apply them while calculating the flux at the boundary face of a control volume. The second method is more direct by working with the coefficients in the discretized equation such that the boundary conditions are satisfied. The second method is followed in the present work.

3.4.2 Solid domain

Consider the stress vector σ_n on an oblique plane P with unit normal \mathbf{n} through point O of a medium as shown in Figure 3.3. The boundary conditions for the solid domain can be expressed as

$$\sigma_s \cdot \mathbf{n} = \mathbf{f} \tag{3.14}$$

where the unit normal vector to the plane is defined as

$$\boldsymbol{n} = \boldsymbol{i}n_x + \boldsymbol{j}n_y + \boldsymbol{k}n_z \tag{3.15}$$

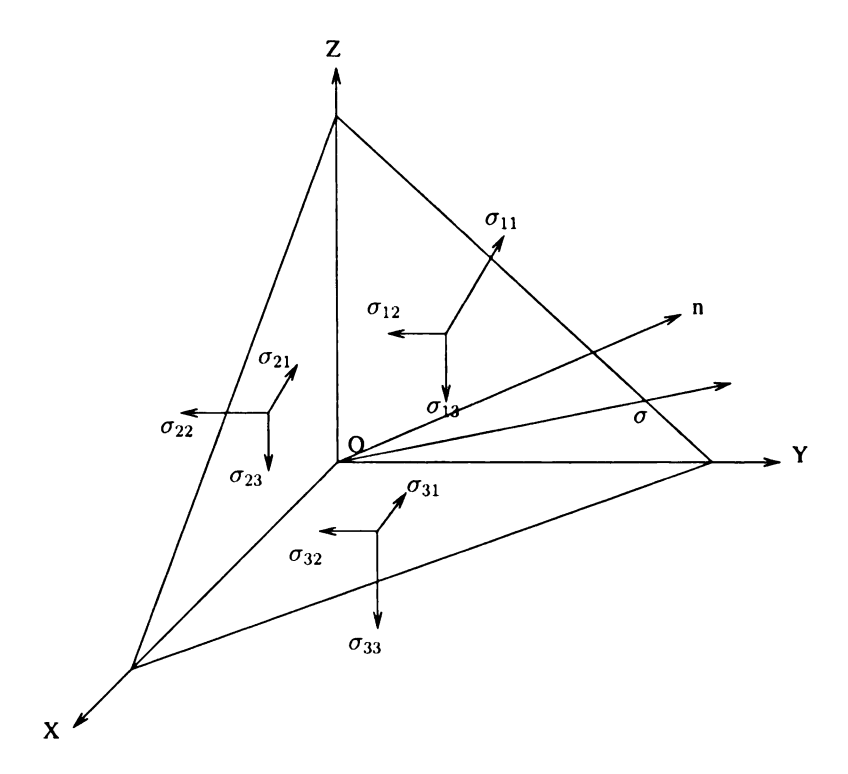


Figure 3.3. Stress on an oblique plane

with n_i as the directional cosines of the unit vector \boldsymbol{n} relative to axes (X, Y, Z).

By definition, the stress vector σ_n may be represented in terms of its (X, Y, Z) projections. Hence

$$\boldsymbol{\sigma}_{n} = \boldsymbol{i}\sigma_{nx} + \boldsymbol{j}\sigma_{ny} + \boldsymbol{k}\sigma_{nz} \tag{3.16}$$

where σ_{nx} , σ_{ny} , and σ_{nz} are the (X, Y, Z) projections of the vector $\boldsymbol{\sigma}_n$. Consequently, we have

$$\sigma_{nx} = n_x \sigma_{xx} + n_y \sigma_{xy} + n_z \sigma_{xz}$$

$$\sigma_{ny} = n_x \sigma_{yx} + n_y \sigma_{yy} + n_z \sigma_{yz}$$

$$\sigma_{nz} = n_x \sigma_{zx} + n_y \sigma_{zy} + n_z \sigma_{zz}$$

$$(3.17)$$

Equations 3.17 represent the components of stress at a point O on an oblique plane P (whose unit normal has direction n) in terms of the six components of stress σ_{ij} ($\sigma_{ij} = \sigma_{ji}$). If point O, is in the surface bounding a medium, and if plane P is tangent to the surface at point O, Equations 3.17 are the stress boundary conditions at point O in terms of the stress components. Substitution of Equation 2.9 into Equations 3.17 yields the boundary condition equations in terms of grid variables.

3.5 Solution Methodology

The conservation equations which are needed to be solved in order to get the flow field and the stress field in the entire domain are the

- Unified Momentum equation (For the entire domain)
- Continuity equation (For the fluid domain)

Solution of the Navier-Stokes equations is complicated by the lack of an independent equation for the pressure, whose gradient contributed to each of the three momentum equations. Furthermore, the continuity equations does not have a dominant variable in incompressible flows. This is not however the case for solid domain. Since there is no pressure term involved in the conservation of momentum (or unified momentum flux terms), this complication is avoided and it is enough that the conservation of momentum equation alone is solved to obtain the displacement of the velocity field. However a solution procedure which can accommodate these differences between the domains and successfully solve for the field variables is extremely critical.

The pressure correction method is one solution where the momentum equations are solved with a guessed pressure field and then, the pressure field is corrected so as to guarantee satisfaction of the continuity equation. This method of solution allowing to separate the momentum and the continuity equations helps in coping with the differences between the domains. In the present work a modified form of SIMPLE (Semi Implicit Method for Pressure Linked Equations) is employed in order to solve the unified momentum and the continuity equations.

The discretized set of unified momentum equations can be represented as

$$a_P \ u_P^{n+1} = \sum_{nb} \ a_{nb} \ u_{nb}^{n+1} + S_u \tag{3.18}$$

where P is the index of the center of the control volume and nb denotes the centers of the neighboring cells that appear in the discretized unified momentum equation. S represents the source term which can be either computed with the known variables at time level n or can be guessed variables such as pressure. The appearance of pressure in the Equation 3.18 depends on whether the fluid region appears at the control volume and does not appear if the control volume is entirely in the solid domain.

Due to the non-linearity and coupling of the underlying differential equations, the Equations 3.18 need to be solved iteratively. Since the computation is done for an unsteady flow, iteration must be continued within each time step.

The solution begins with initializing variables and assuming an initial pressure field for the fluid domain. Then, the unified momentum equations are solved sequentially i.e.., the set of algebraic equations for each component of the momentum is solved in turn, treating the grid point values of its dominant velocity component as the sole set of unknowns. Since the pressure used at fluid control volumes in these iterations was obtained from the previous time step, the velocities computed from Equations 3.18 do not normally satisfy the discretized continuity equation. To enforce the continuity condition, the velocities need to be corrected; this requires correcting the pressure field which is described further. Since the velocities in fluid and solid domains are interdependent on each other once the velocities in are corrected it is necessary to make sure that the solution satisfies both the unified momentum and the continuity equation. Hence this iterative process is carried until both the unified momentum equation and the continuity equation are simultaneously satisfied.

The velocity at node P, obtained by solving the linearized momentum equations (3.18) can be formally expressed as:

$$u_P^{m*} = \frac{S_u^{m-1} - \sum_{nb} a_{nb}^u u_{nb}^{m*}}{a_P^u}$$
 (3.19)

where m indicates the outer iterations which are iterations within one time step. u_P^{m*} is not the final value of the velocity for iteration m; it is predicted value as indicated by the asterisk (*). The corrected final values should satisfy the continuity equation

for the liquid domain. Hence the next step is to solve the pressure correction equation (continuity equation). Since the Equation 3.20 is required only for the liquid domain, the pressure correction in the solid domain is taken as zero.

$$a_P^p p_P' = \Sigma_{nb} a_{nb}^p p_{nb}' + S_p'$$
 (3.20)

where the coefficients a^p are evaluated based on u^{m*} . Once the pressure correction is known, the correct pressure field may be obtained using formula (3.21).

$$p^{m} = p^{m-1} + \alpha p' \tag{3.21}$$

and the corresponding corrected velocities are calculated using

$$u_{P}^{m} = u_{P}^{m*} + u_{P}^{'} \qquad where \qquad u_{P}^{'} = d_{P}(\Delta p')_{P}$$
 (3.22)

where d is given from Equation 3.13. The new velocity field at the new iteration remains unchanged for the solid domain as the pressure correction is zero in the solid domain. However u_P^m in the liquid domain satisfies the continuity condition, but the velocity and pressure fields do not satisfy the unified momentum equations simultaneously. Hence a new outer iteration and the process is continued until a velocity field which satisfies both the unified momentum and continuity equations is obtained.

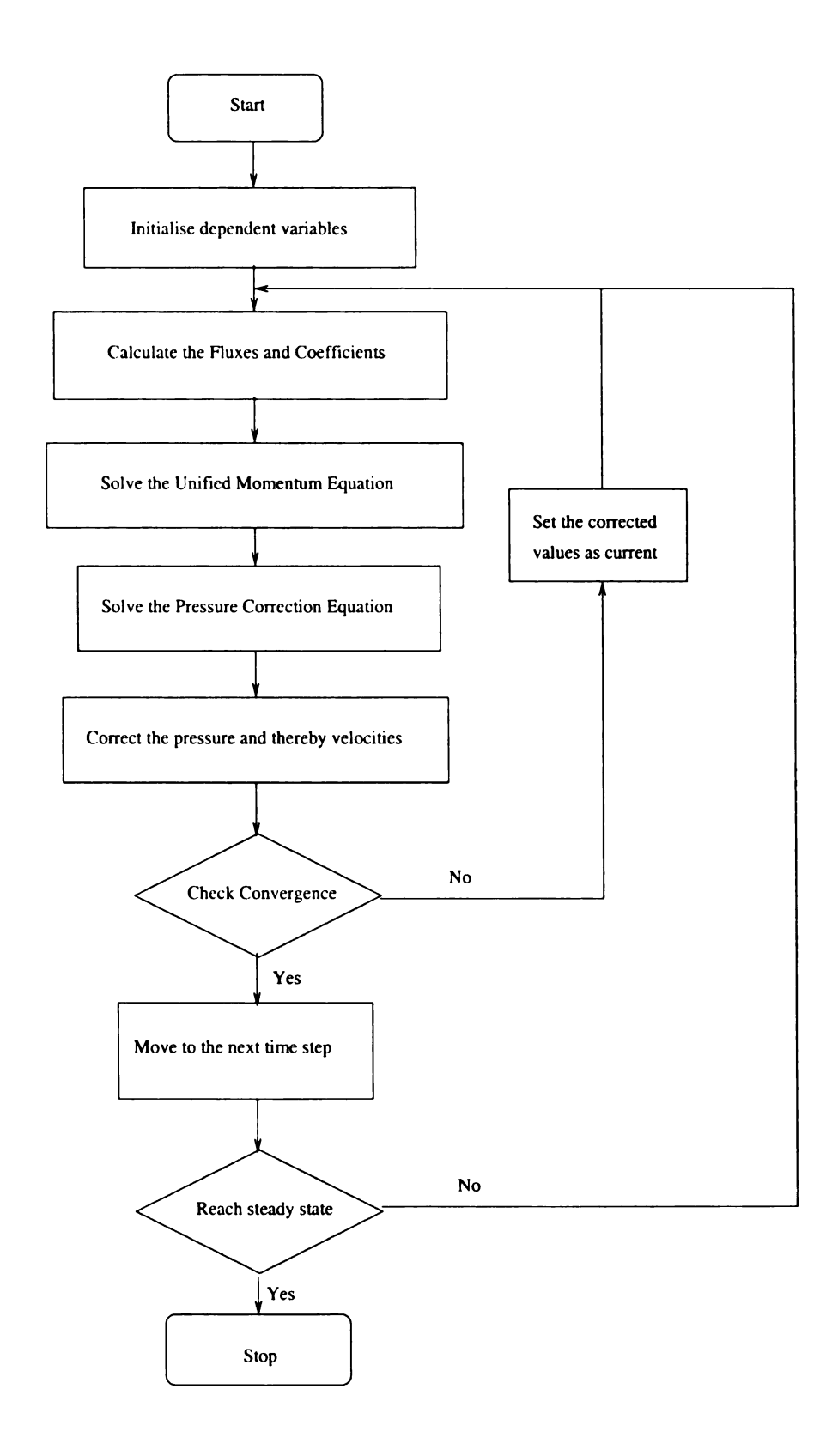


Figure 3.4. Flow chart of the solution procedure

CHAPTER 4

Numerical Tests

The objective of this section is to discuss the accuracy, efficiency and versatility of the unified momentum approach explained in the previous sections by means of numerical examples. In the first example, a flow between two parallel plates is considered. The objective of this analysis is to solve for both the flow field and the stresses observed in the plates simultaneously. However due to the symmetry, the resultant stress field is shown only for the bottom plate. The results obtained from the numerical method are compared with the results from ABAQUS. The second example is a driven cavity problem where the objective is study the interaction between the fluid flow and the stresses in the container holding the fluid. Unlike the poiseuille flow, the interaction between the fluid and the container is more complex and dynamic. Images in this thesis are presented in color.

4.1 Poiseuille flow

Poiseuille flow is one of the most commonly observed phenomenon. One of it's main applications is study of blood flow in arteries. Poiseuille flow can be described as the flow of a viscous fluid in a channel. The setting is described in the Figure 4.1. The fluid flows between two parallel plates which are $0.04 \ m$ apart and $0.3 \ m$ in length. Each of the plates itself is $0.04 \ m$ wide and $0.3 \ m$ in length. The plates are supported by rollers on all the remaining sides other than the fluid. A pressure gradient is applied at the ends of the channel. The pressure at the intake is $30 \ Pa$ while it is $1 \ Pa$ at the outlet.

The fluid in the channel is modeled as water with a density of $1000~Kg/m^3$ and a viscosity of $2.00 \times 10^{-2}~N/m^2$. The bottom plate material is considered as steel with a density of 7860 Kg/m^3 , Young's Modulus of $2.03 \times 10^{11}~N/m^2$ and Poisson ratio of 0.33.

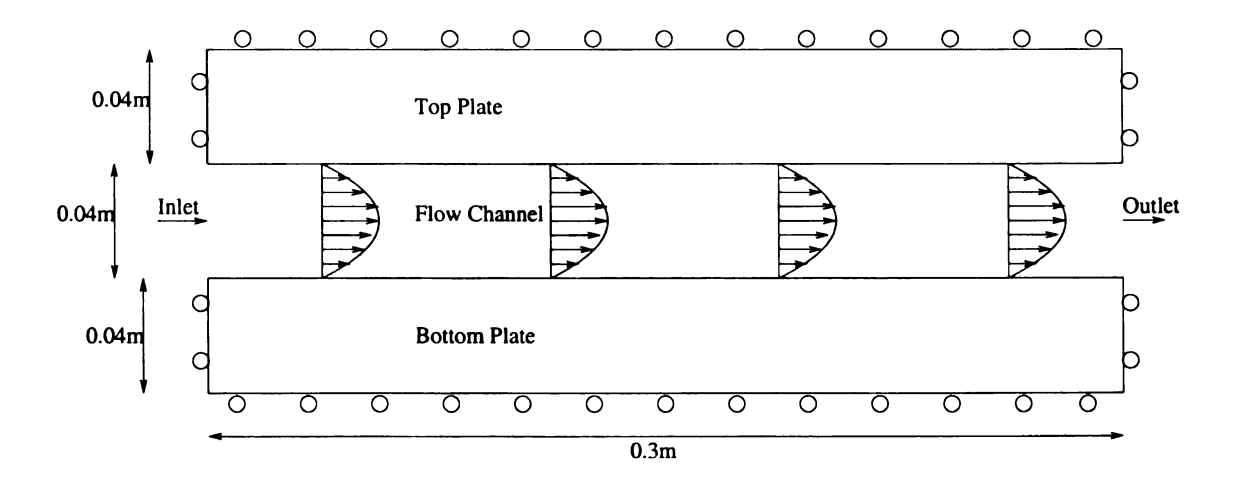


Figure 4.1. Poiseuille flow between parallel plates

4.1.1 Validation

The validation solution for the problem is computed assuming steady state conditions $(\partial u/\partial t = 0)$. The no-slip boundary condition at the top and bottom edges of the channel reads u = 0. Since the viscous forces should balance the pressure force we have,

$$\mu \frac{\partial^2 u}{\partial y^2} = \frac{\partial p}{\partial x} \tag{4.1}$$

Integrating twice and imposing the boundary conditions we obtain

$$u(y) = \frac{1}{2\mu} \frac{\Delta p}{l} \left[(a/2)^2 - y^2 \right]$$
 (4.2)

where a is the width of the channel in the y-direction, and l is the length in the x-direction.

The velocity profile given by Equation 4.2 is a parabola, with the fluid in the center of the channel having the highest speed. With the velocity profile known, the stresses acting on the plate can be calculated from the Equation 2.3 as

$$\sigma_{xx} = -p$$

$$\sigma_{yy} = -p$$

$$\sigma_{xy} = \mu(\frac{\partial u}{\partial y})$$
(4.3)

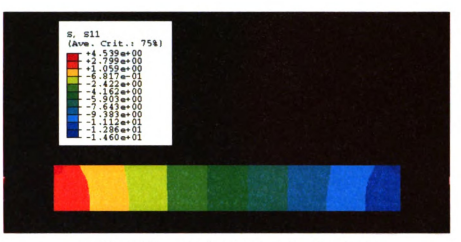
Hence the shear stress acting on the plates is calculated from the Equations 4.3 and 4.2, which is obtained as 2 Pa. This along with the normal stresses are then applied on the plates using ABAQUS. Due to the symmetry of the problem only the bottom

plate is further considered for the stress analysis. The top surface of the plate is loaded with shear stress and normal stress obtained from the analytical solution of Poiseuille flow. The plate is modeled as a 2-Dimensional deformable part with 200*200 grid points in the mesh. A static solver is used to obtain the equilibrium stress distribution in the plate in ABAQUS. The results are shown in the Figure 4.2. The normal stress in the x-direction (Figure 4.2(a)) has a maximum value of 4.5 Pa and a minimum value of -14.6 Pa. The normal stress in the y-direction (Figure 4.2(b)) has a very similar pattern to the pressure in the fluid flow as it is very less affected by the shear stress acting on the top of the plate. The shear stress (Figure 4.2(c)) however varies from a maximum of 1.9 Pa at the top surface to 0 Pa at the bottom surface.

4.1.2 Numerical Results

The numerical model is implemented in FORTRAN 90 with 200 *200 grid on a single processor machine with Intel Pentium 4 3.20 GHz processor. The running time for the entire simulation is approximately 8 hrs. A Line TDMA (Tri Diagonal Matrix Algorithm) solver is employed to solve the inner iteration for individual velocity components and the pressure corrections.

Considering the normal stress in the x-direction at different intermediate times shown in the Figure 4.3, the subtle variations in the stress field inside the solid can be noticed. The variations in the stresses inside the fluid region are very less as it is dominated by the pressure which reaches equilibrium pretty quickly. Initially the



(a) Normal Stress in the plate in x-direction (σ_{xx})



(b) Normal Stress in the plate in y-direction (σ_{yy})



(c) Shear Stress in the plate (σ_{xy})

Figure 4.2. Steady state stress distribution in the solid from ABAQUS

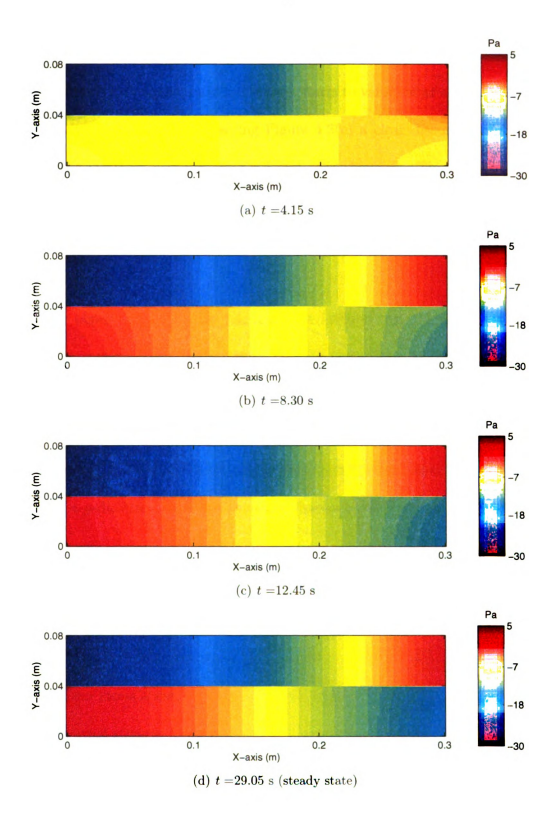


Figure 4.3. Normal stress distribution in x-direction (σ_{xx}) at different time intervals

stress remains uniform in the solid plate, however as the flow develops and the shear stress increases the normal stress in x-direction starts to vary and at a time of 29.05 s reaches steady state. Also by observing Figure 4.3(c) a clear discontinuity can be noticed at the interface between the fluid and solid domains. This is as expected since the normal to the interface is in the y-direction whereas the stress which is being considered is in x-direction.

However, by observing the Figure 4.4, it can be inferred that the normal stress in y-direction is continuous at the interface in both the phases, which is very much in accordance with the interface boundary conditions. The normal stress in the y-direction is very less affected by the flow development and increase in the shear stress as the shear stress (2 Pa) is considerably small with respect to the normal stresses in the y-direction acting on the plate due to the fluid flow.

The variations in the shear stress inside the fluid and solid region can be noticed from the Figure 4.5. Initially at time 4.15 s (Figure 4.5(a)), the shear stress in the fluid region is negligibly small due to the very low velocities while there is a slight amount of shear stress shown as circular regions at the side ends in the solid region due to the normal stresses inside the solid region. As time progresses these circular patterns inside the solid region tend to merge as can be observed from Figure 4.5(b) and finally as the flow develops and the shear stress increases in the fluid region the shear stress in the plate tends to stabilize and reach its steady state (Figure 4.5(d)).

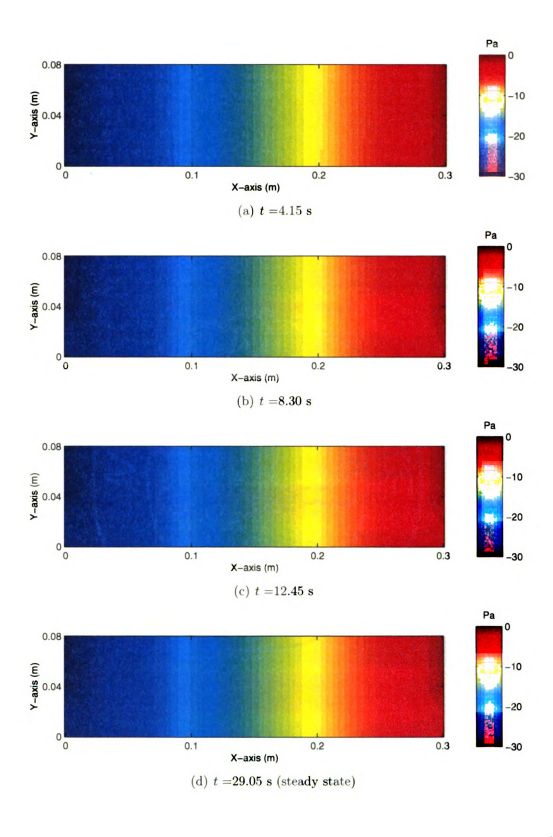


Figure 4.4. Normal stress distribution in y-direction (σ_{yy}) at different time intervals

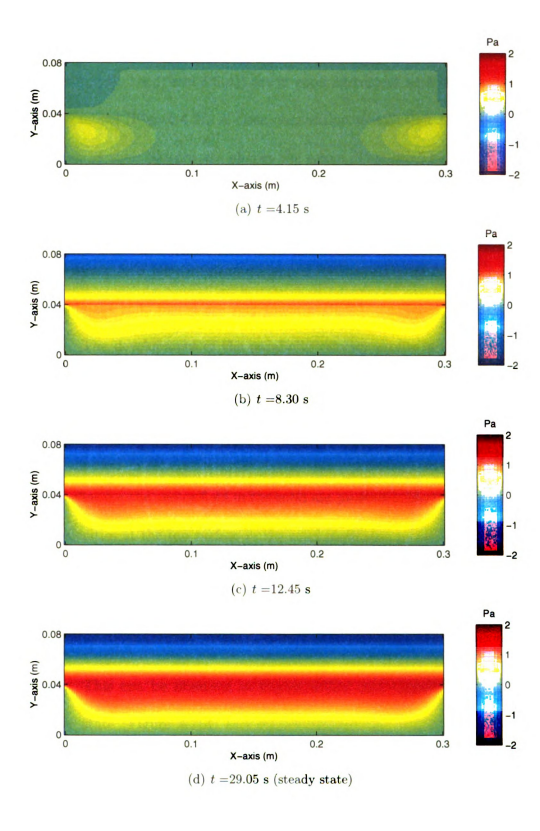


Figure 4.5. Shear stress distribution (σ_{xy}) at different time intervals

The stresses in the plate at the steady state obtained from the numerical results (Figures 4.3(d), 4.4(d) and 4.5(d)) are in good agreement with the results from the ABAQUS model (Figure 4.2). A close observation reveals that the order of the stresses as well as their pattern are almost the same. This provides the validation for the current proposed model.

The velocity vector field for the entire domain is shown in Figure 4.6. As expected the velocities in the solid region are very much negligible compared to those in the fluid domain. The development of the parabolic velocity profile in the fluid region can be noticed, which agrees with the analytical result derived for the Poiseuille flow.

As the orders of the velocities in fluid and solid domains are very different, a different set of images showing the vector field in the solid are presented (Figure 4.7). At time $4.15 \, s$, the velocities at the top surface in the solid plate tend to go down due to the sudden increase in the pressure initially which can be observed from Figure 4.7(a) as well as Figure 4.8(a), however this tendency decreases and the vertical component of the velocities tend to decrease as time progresses and the pressure becomes more steady. This can be observed in Figure 4.8(b) and Figure 4.8(c). Finally at the steady state (Figure 4.7(d) and Figure 4.8(d)), the velocities in the plate become zero due to which there are no streamlines in the solid region in Figure 4.8(d).

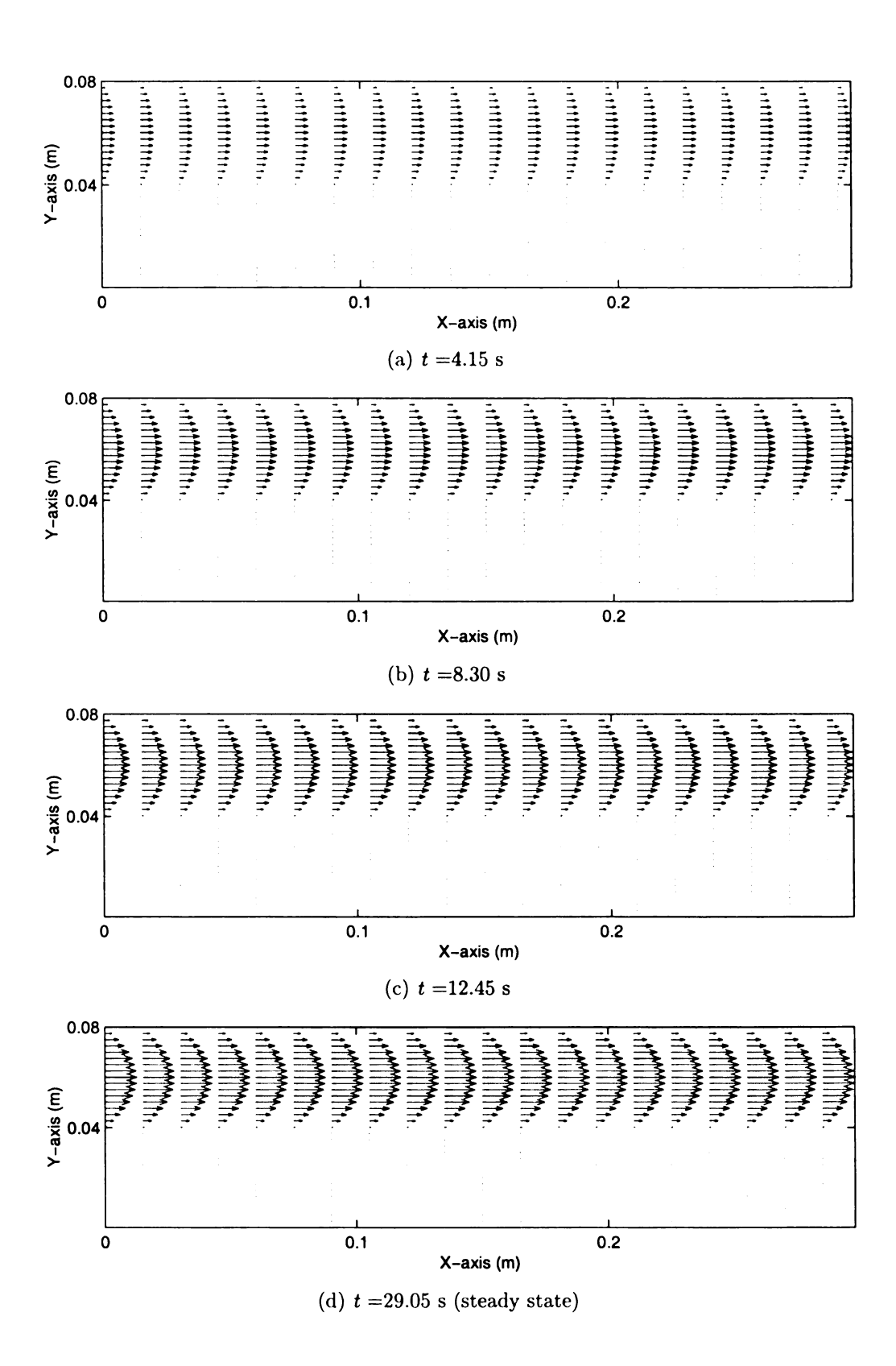


Figure 4.6. Velocity vector field in the fluid at different time intervals

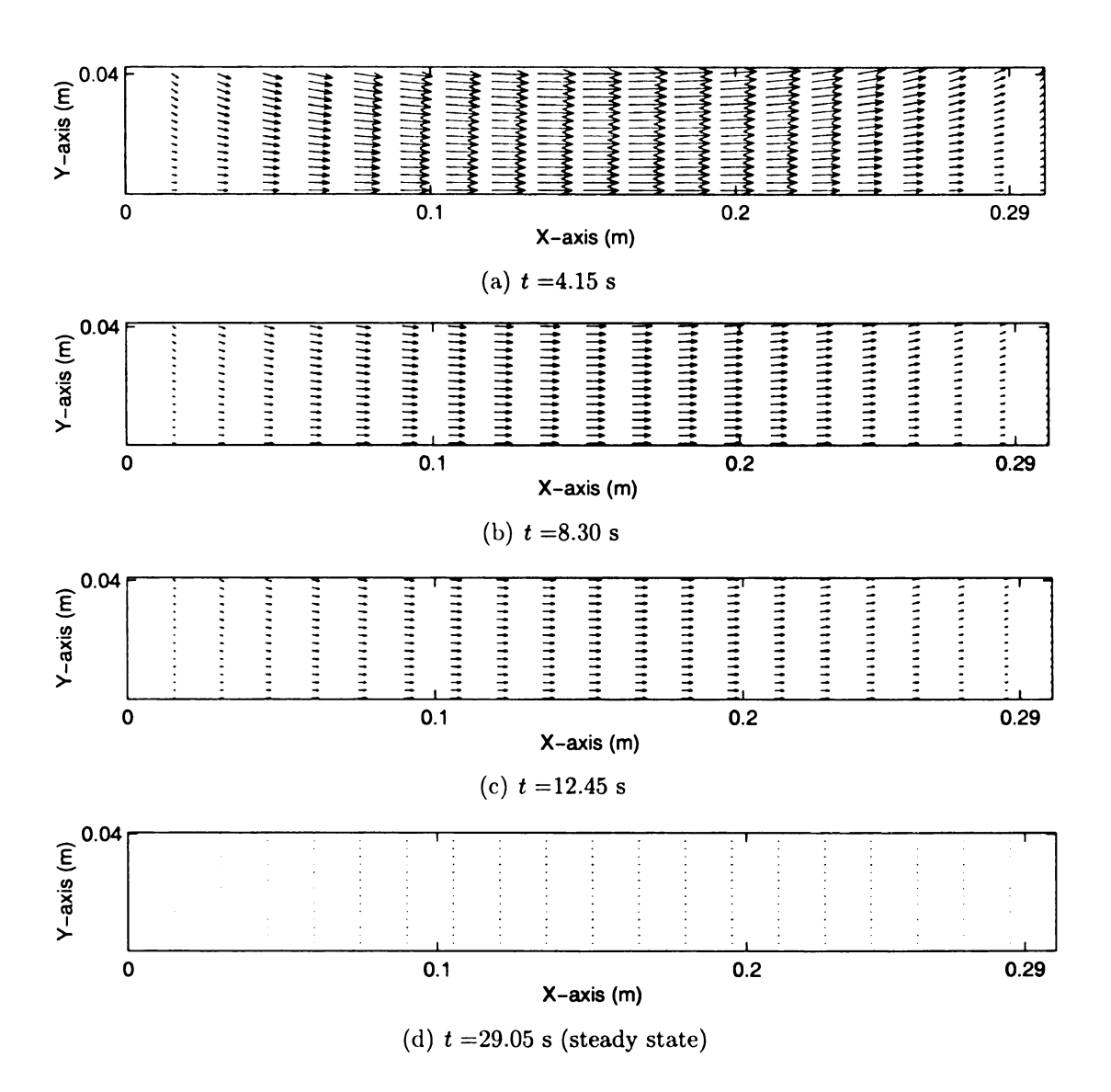


Figure 4.7. Velocity vector field in the solid at different time intervals

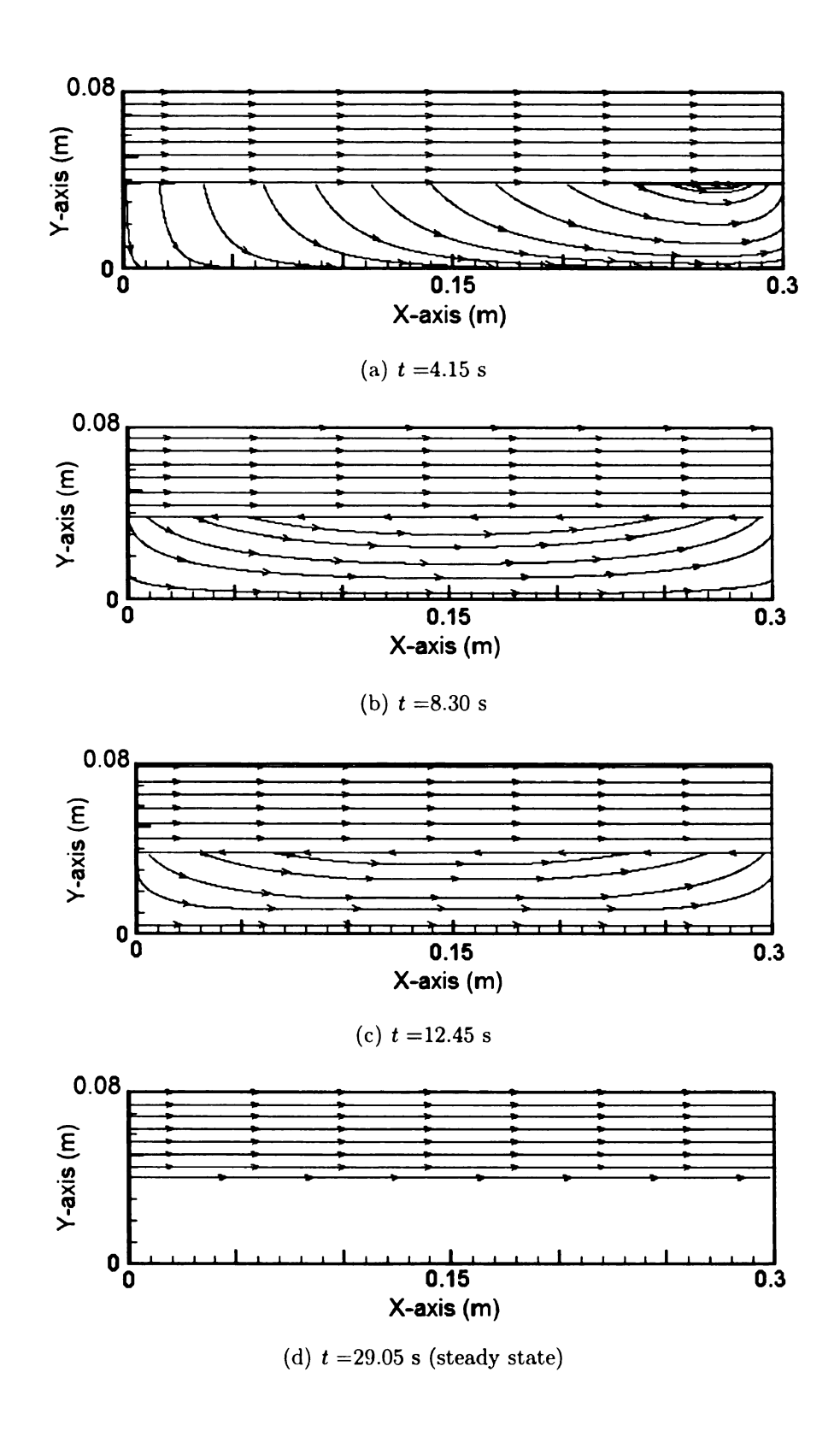


Figure 4.8. Stream lines at different time intervals

4.2 Driven Cavity Problem

The Driven Cavity problem is one of the common benchmark problems in CFD literature. The schematic model of the present problem is shown in Figure 4.9. As in the case of Poiseuille flow, the driven cavity problem also has a fluid flow inside a solid container. The dimensions of the cavity in the container are $0.07 m \times 0.07 m$ whereas those of the container are $0.14 m \times 0.14 m$. The top layer of the fluid flow is driven by a lid at a constant velocity of 0.05 m/s due to which flow in induced inside the fluid region. The flow induces pressure (stresses) which in turn act on the metal container holding the fluid creating stresses in the container.

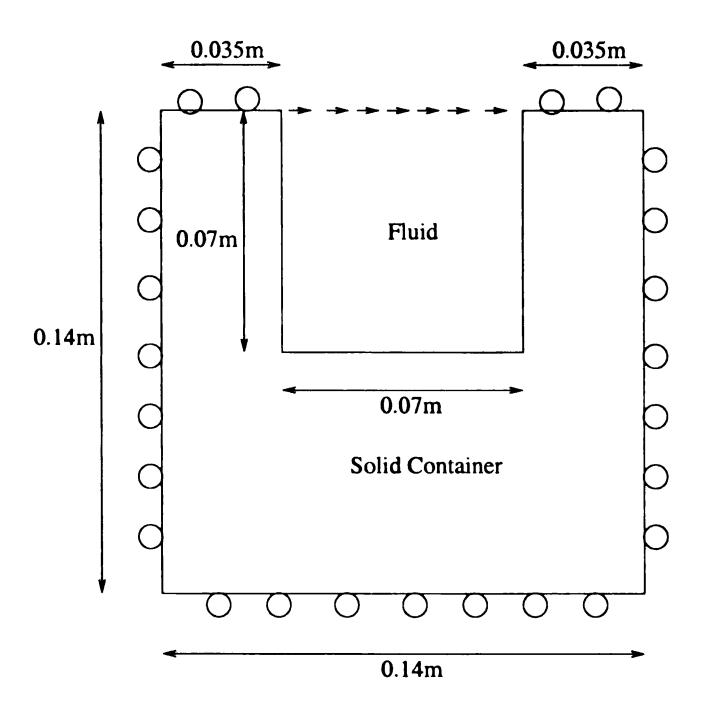


Figure 4.9. Schematic representation of driven cavity flow

The fluid in the channel is modeled as water with a density of 1000 Kg/m^3 and a

viscosity of $6.00 \times 10^{-3} \ N/m^2$. The bottom plate material is considered as steel with a density of 7860 Kg/m^3 , Young's Modulus of $2.03 \times 10^{11} \ N/m^2$ and Poisson ratio of 0.33.

4.2.1 Numerical Results

The numerical model is implemented in FORTRAN 90 with 200 * 200 grid on a single processor machine with Intel Pentium 4 3.20 GHz processor. The running time for the entire simulation is approximately 6.5 hrs. A Line TDMA solver is employed to solve the inner iteration for individual velocity components and the pressure corrections. The results are shown below.

The normal stresses in x-direction inside the domain are shown in Figure 4.10. Initially, the normal stresses in x-direction are very much symmetric concentrated heavily at the top left and right corners of the fluid-structure interface (Figure 4.15(a)). As time progresses, the stresses become more biased towards the top right corner of the interface due to the flow direction. The beginning of the formation of a vortex can be observed from Figure 4.15(b) to Figure 4.10(h), during which the pressure field inside the fluid flow varies. This variation results in the change of the stress pattern inside the solid domain which can be noticed as the increase of the stresses at the bottom portion of the solid container. The normal stresses in x-direction inside the solid domain are a little higher in magnitude at the right end because of

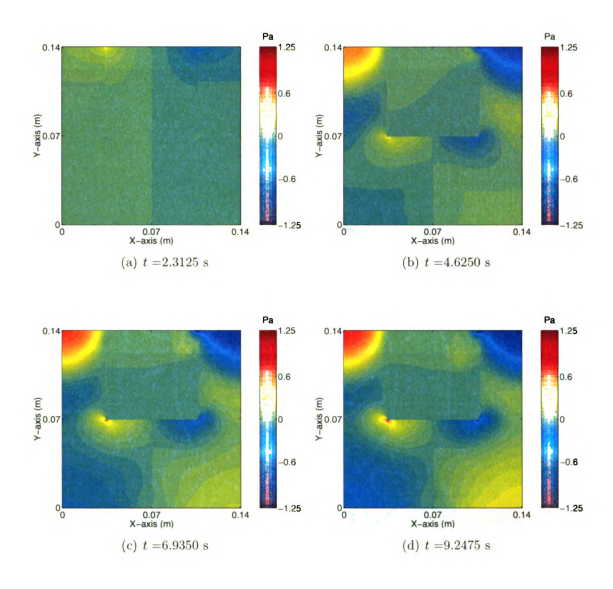


Figure 4.10. Normal stress distribution in x-direction (σ_{xx}) at different time intervals

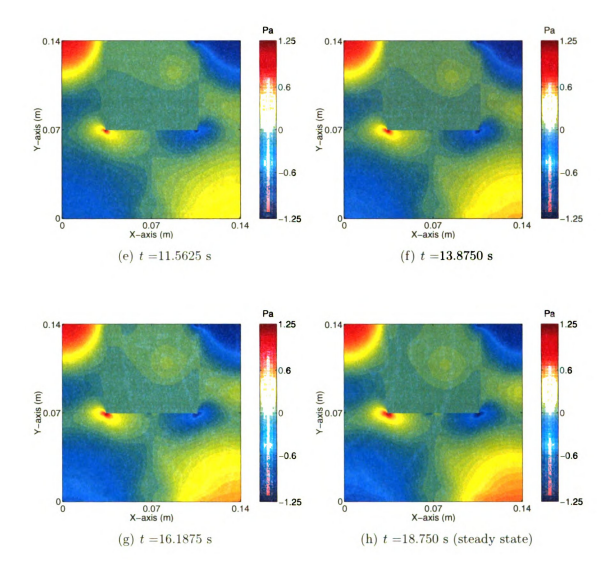


Figure 4.10. Cont'd

the direction of flow pattern which is as expected. Also, the continuity of the normal stress in the x-direction can be observed at the left and right interfaces and not at the bottom interface which is in accordance with the interface boundary conditions.

The normal stresses in y-direction inside the domain are shown in Figure 4.11. The variations in the normal stresses in y-direction follow very much the same pattern as the normal stresses in x-direction. Stresses are symmetric at the initial stages (Figure 4.11(a)) and as time progresses, the they become more pronounced. The beginning of the formation of a vortex can be observed from Figure 4.11(b) to Figure 4.11(h), during which the change of the stress pattern inside the solid domain which can be noticed as the increase in the stresses at the bottom portion of the solid container. However one important difference between the normal stresses in x and y directions is that the normal stresses in y direction (Figure 4.11) are continuous across the bottom interface whereas the normal stresses in x direction (Figure 4.10) are continuous across the left and right interfaces.

The shear stresses inside the domain are shown in Figure 4.12. Initially, the shear stresses (Figure 4.12(a)) in the entire domain are negligible as the flow is still undeveloped, however the shear stress patterns become more pronounced in the later stages. Inside the fluid domain (Figure 4.12(b) to Figure 4.12(h)) we have a higher shear stress at the top layer and at the top right interface where the velocity gradients are high. This results in a higher shear stress in the right side of solid domain compared to that in the left region. The formation of the circular region in

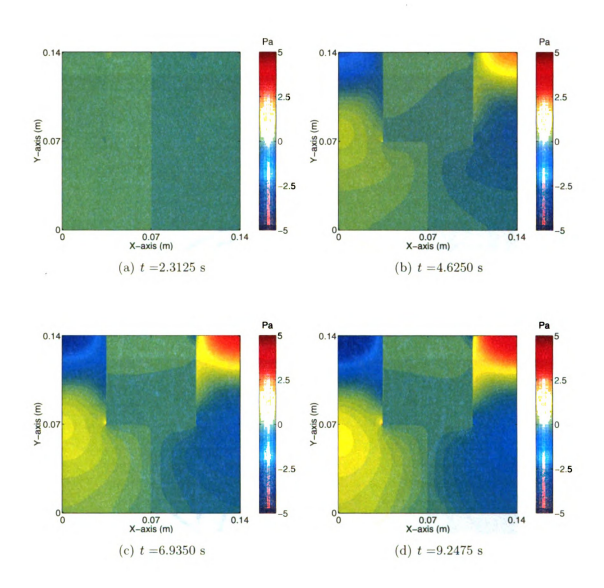


Figure 4.11. Normal stress distribution in y-direction (σ_{yy}) at different time intervals

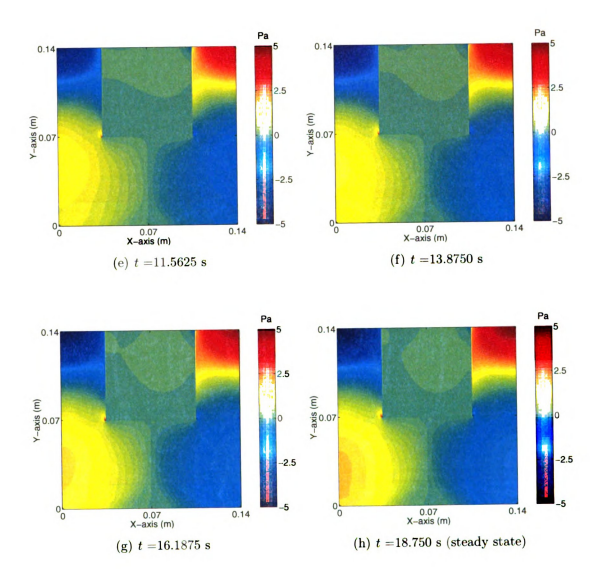


Figure 4.11. Cont'd

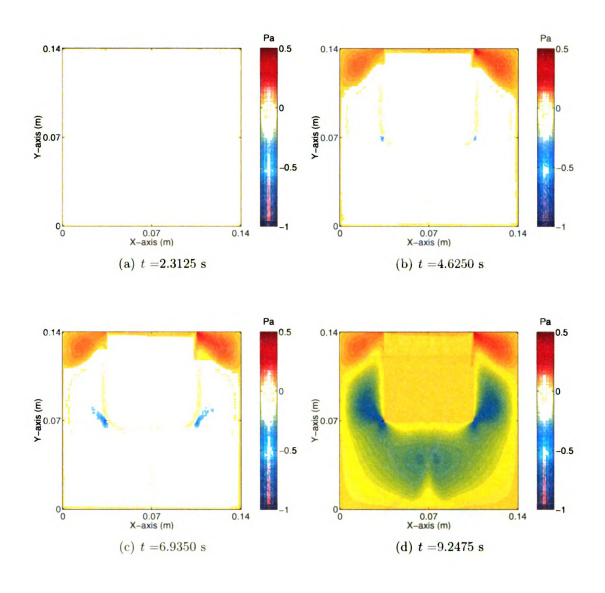


Figure 4.12. Shear stress distribution (σ_{xy}) in the container at different time intervals

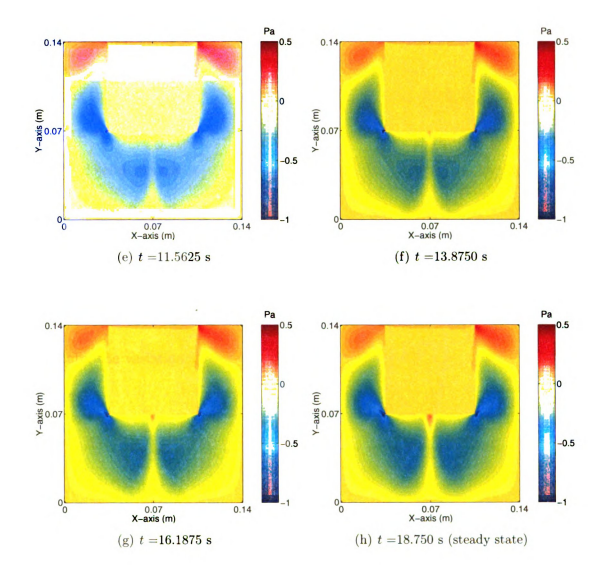


Figure 4.12. Cont'd

the bottom region of the container observed in Figure 4.12(b) and Figure 4.12(c) can be explained from the fact that the solid particles tend to move in a circular mode at these stages. Later as the velocities of the solid region become more flat, this circular region separates into two halves as can be noticed in Figure 4.12(d) to Figure 4.12(h).

Considering the velocity vector fields (Figures 4.13 and 4.14) and streamlines (Figure 4.15) shown at different time intervals, it can be inferred that the particles in both the fluid and solid regions have a similar velocity pattern at the initial stages. As the flow develops it can be observed that the velocities in the solid tend to decrease and the streamlines become more and more flat while the velocities in the fluid region tend to develop further. This is due to the fact that velocities inside the solid region are dependent on the rate of change of pressure at the interface. As the flow reaches steady state, the variation in the pressure field decreases and hence solid velocities become zero.

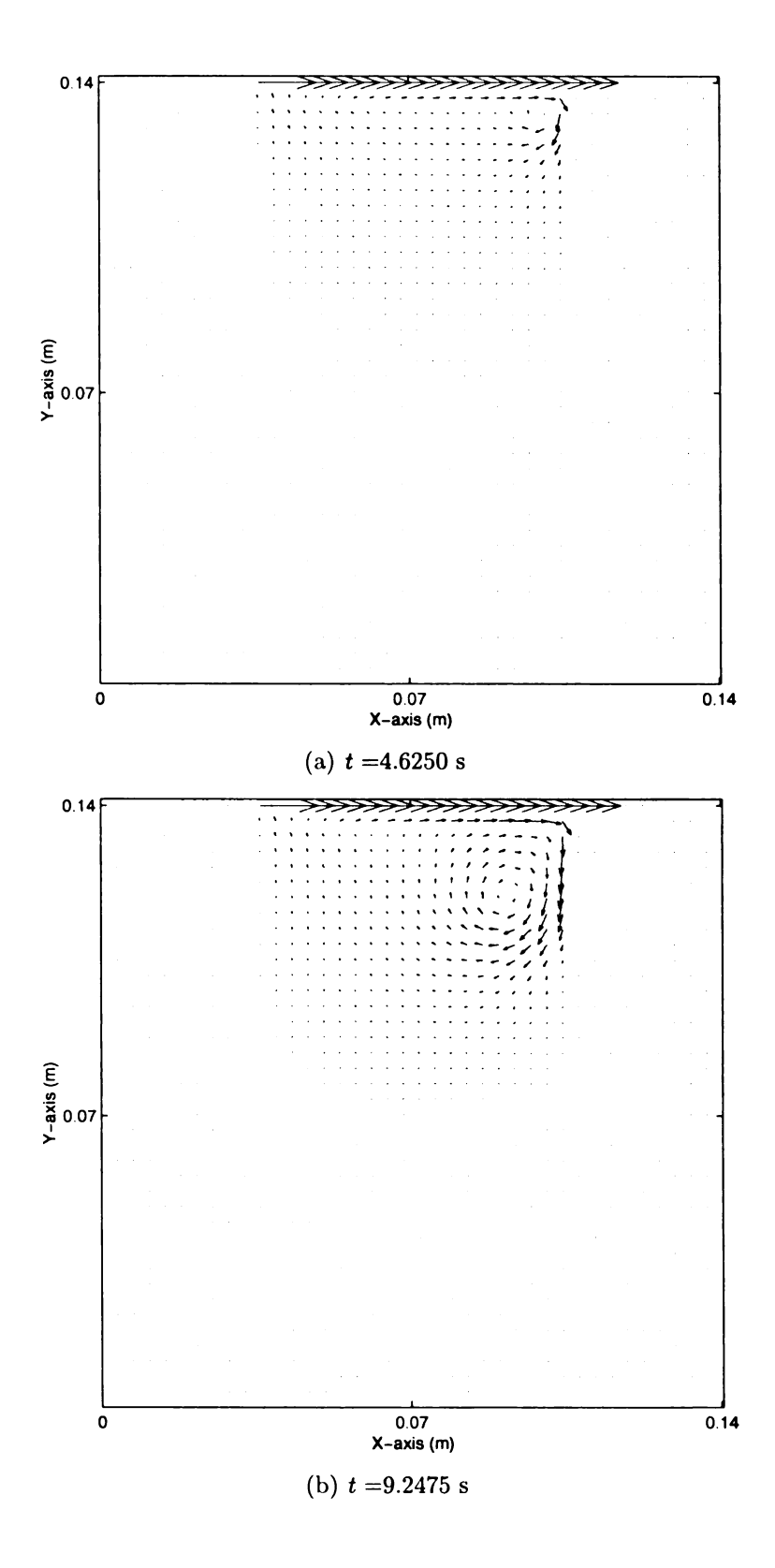


Figure 4.13. Velocity vector field in the fluid at different time intervals

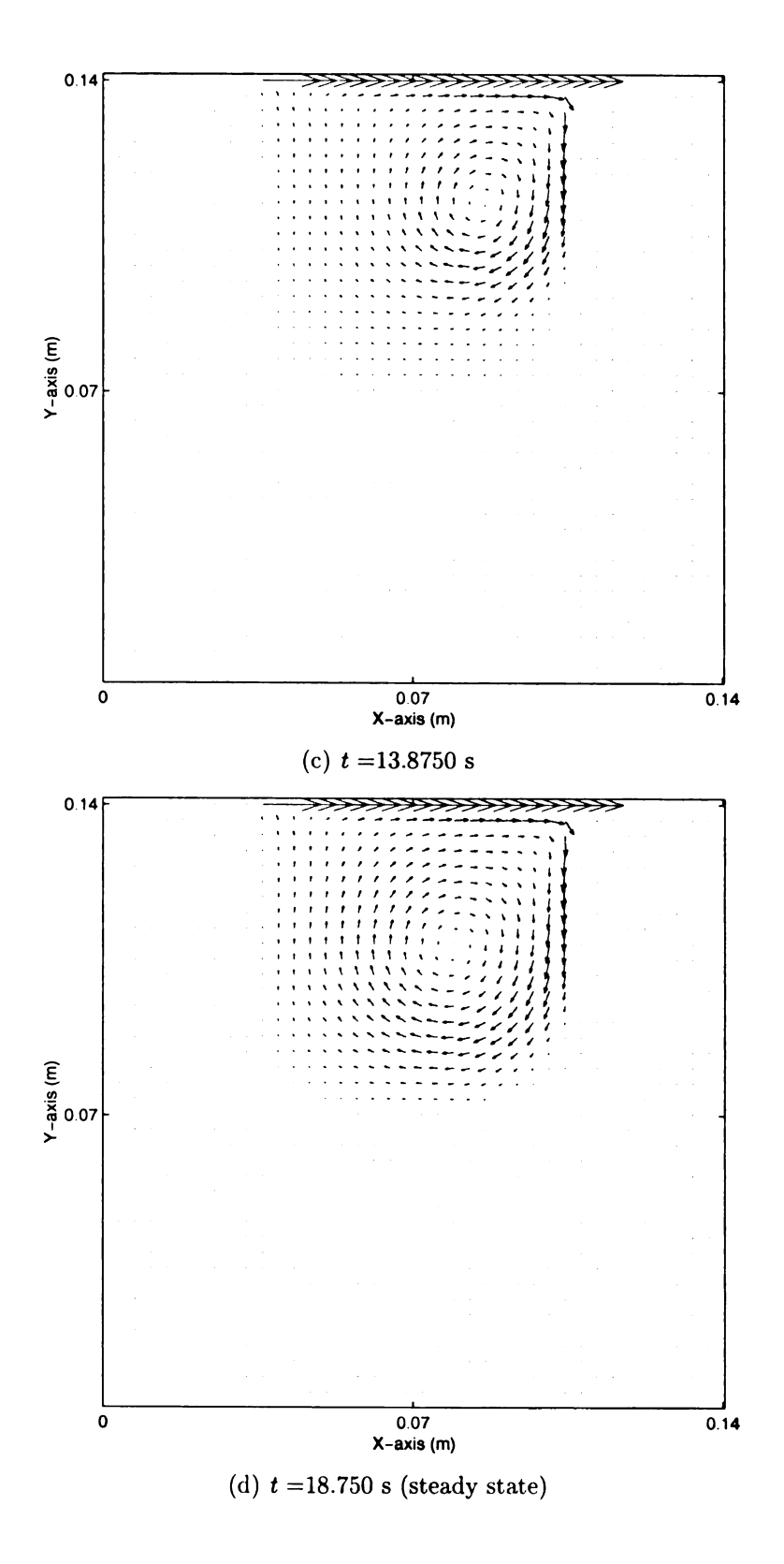


Figure 4.13. Cont'd

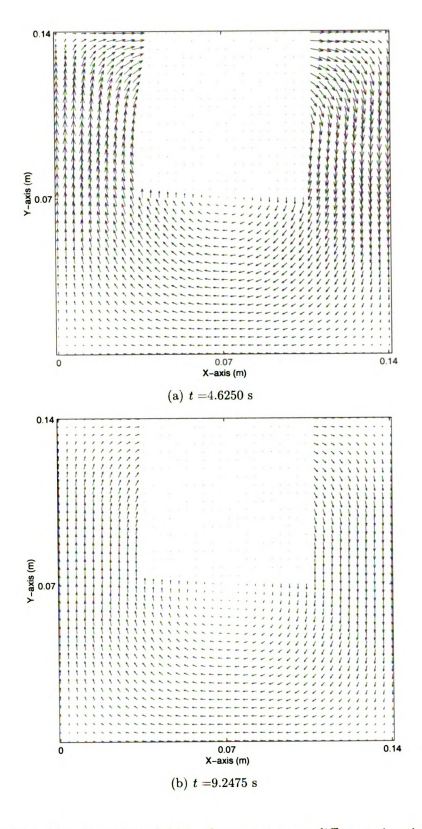


Figure 4.14. Velocity vector field in the container at different time intervals

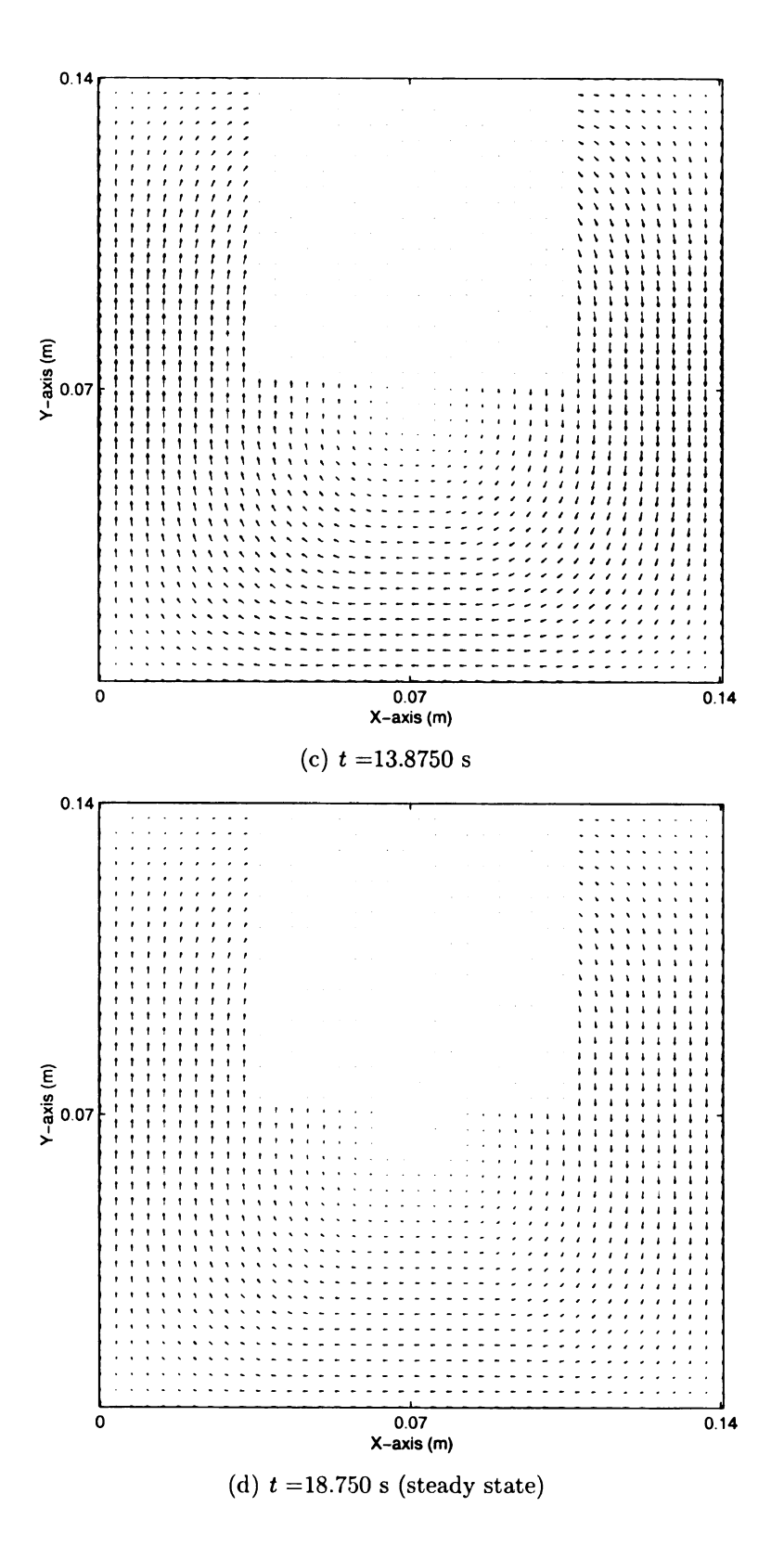


Figure 4.14. Cont'd

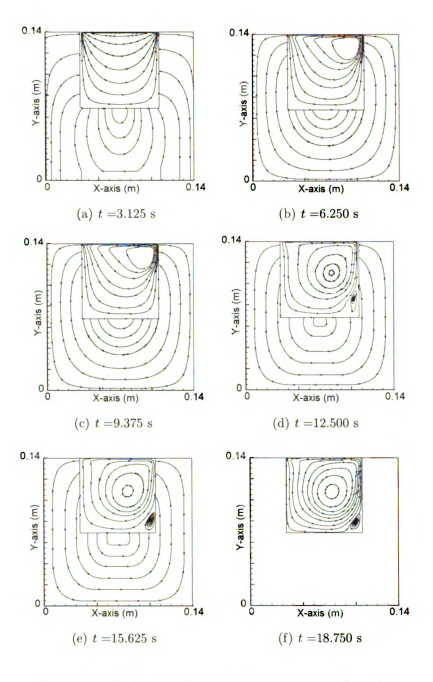


Figure 4.15. Stream lines at different time intervals

CHAPTER 5

Conclusion

A unified momentum equation approach is developed in this work to solve the fluid-structure interaction problems, using a uniform and consistent spatial and temporal discretization through out the domain along with a mechanism to interact among the phases freely without any interfacing algorithms. This model combines the advantages of having the same governing equations in both the phases along with the finite volume approach to solve the fluid-structure interaction problems. The main advantages include:

- Treating the fluid and solid domains as a whole which means that a single numerical algorithm can be applied to both phases
- No boundary conditions required at the fluid-structure interface as they are inherently taken care of the force balance formulation
- Interpolation of data from one phase to another not required as the grid is continuous with velocities as the field-variables for both the phases.

• Coupling of separate system of equations for solid and liquid not required thereby avoiding the formation of ill-conditioned system of equations.

The method is then tested for different problems involving fluid-structure interactions. First, it is applied to a flow between two parallel plates where stresses are induced in the plates due to the flow field inside. The numerical results are then compared with analytical results obtained from traditional approach of solving the fluid and structural dynamics separately. The analytical solution for the fluid flow is used as input for the ABAQUS model to obtain the stresses in the plates. Both the numerical and the analytical results show good agreement with each other. Not only the pattern and order of the stress field in the two results are quite close to each other but also the continuity of the stresses in the normal direction is also satisfied at the interface. The model is further successfully applied to the lid driven cavity problem to determine the flow field and the stress distribution in the container simultaneously.

CHAPTER 6

Future Work

This chapter describes how the present work can be extended to further improve it.

- The present model needs to be extended to problems in which the solid-fluid interfaces intersect the computational-cell walls obliquely
- Even though the validation of the proposed model is established with the poiseuille flow, several other problems need to be studied and compared with the experimental results to fully establish the accuracy of the method in predicting the stresses for several other fluid-structure interaction problems
- The present model needs to be further extended to include the energy equation so that the thermal and phase transformations in the domain can also be captured simultaneously in both the phases
- Developing a more robust model allowing interface movement and boundary displacement in the solid domain

• Improvements to make the present numerical method more efficient and accu-						
rate need to be further developed.						

BIBLIOGRAPHY

BIBLIOGRAPHY

- [1] F.P.T. Baaijens. A fictitious domain/mortar element method for fluid-structure interaction. *International Journal for Numerical Methods in Fluids*, 35(7):743 761, 2001.
- [2] Klaus-Jurgen Bathe and Hou Zhang. Finite element developments for general fluid flows with structural interactions. *International Journal for Numerical Methods in Engineering*, 60(1):213 232, 2004.
- [3] O. Bendiksen. New approach to computational aeroelasticity. pages 1712 1732, 1991.
- [4] Oddvar O. Bendiksen. Fluid-structure coupling requirements for time-accurate aeroelastic simulations. American Society of Mechanical Engineers, Aerospace Division (Publication) AD, 53-3:89 104, 1997.
- [5] F. Bertrand, P.A. Tanguy, and F. Thibault. Three-dimensional fictitious domain method for incompressible fluid flow problems. *International Journal for Numerical Methods in Fluids*, 25(6):719 736, 1997.
- [6] Frederic J. Blom. Monolithical fluid-structure interaction algorithm applied to the piston problem. Computer Methods in Applied Mechanics and Engineering, 167(3-4):369 391, 1998.
- [7] A.N. Brooks and T.J.R. Hughes. Streamline upwind/petrov. galerkin formulations for convection dominated flows with particular emphasis on the incompressible navier-stokes equations. Computer Methods in Applied Mechanics and Engineering, pages 199 259, 1990.
- [8] F. Casadei and J.P. Halleux. Algorithm for permanent fluid-structure interaction in explicit transient dynamics. Computer Methods in Applied Mechanics and Engineering, 128(3-4):231 289, 1995.
- [9] F. Casadei, J.P. Halleux, A. Sala, and F. Chille. Transient fluid-structure algorithms for large industrial applications. *Computer Methods in Applied Mechanics and Engineering*, 190(24-25):3081 3110, 2001.

- [10] Folco Casadei and Serguei Potapov. Permanent fluid-structure interaction with non-conforming interfaces in fast transient dynamics. Computer Methods in Applied Mechanics and Engineering, 193(39-41 SPEC ISS):4157 4194, 2004.
- [11] J. De Hart, G.W.M. Peters, P.J.G. Schreurs, and F.P.T. Baaijens. A three-dimensional computational analysis of fluid-structure interaction in the aortic valve. *Journal of Biomechanics*, 36(1):103 112, 2003.
- [12] J. Donea, S. Giuliani, and J. P. Halleux. Arbitrary lagrangian-eulerian finite element method for transient dynamic fluid-structure interactions. *Computer Methods in Applied Mechanics and Engineering*, 33(1-3):689 723, 1981.
- [13] C. Farhat, M. Lesoinne, and P. LeTallec. Load and motion transfer algorithms for fluid/structure interaction problems with non-matching discrete interfaces: Momentum and energy conservation, optimal discretization and application to aeroelasticity. Computer Methods in Applied Mechanics and Engineering, 157(1-2):95 - 114, 1998.
- [14] Roland Glowinski, Tsorng-Whay Pan, and Jacques Periaux. Fictitious domain method for dirichlet problem and applications. Computer Methods in Applied Mechanics and Engineering, 111(3-4):283 303, 1994.
- [15] Peter Hansbo. Characteristic streamline diffusion method for convection-diffusion problems. Computer Methods in Applied Mechanics and Engineering, 96(2):239 253, 1992.
- [16] Peter Hansbo, Joakim Hermansson, and Thomas Svedberg. Nitsche's method combined with space-time finite elements for ale fluid-structure interaction problems. Computer Methods in Applied Mechanics and Engineering, 193(39-41 SPEC ISS):4195 – 4206, 2004.
- [17] Matthias Heil. An efficient solver for the fully coupled solution of large-displacement fluid-structure interaction problems. Computer Methods in Applied Mechanics and Engineering, 193(1-2):1 23, 2004.
- [18] C. W. Hirt, A. A. Amsden, and J. L. Cook. An arbitrary lagrangian-eulerian computing method for all flow speeds. *Journal of Computational Physics*, 135(2):203 237, 1997.
- [19] Bjorn Hubner, Elmar Walhorn, and Dieter Dinkler. A monolithic approach to fluid-structure interaction using space-time finite elements. Computer Methods in Applied Mechanics and Engineering, 193(23-26):2087 2104, 2004.

- [20] Thomas J. R. Hughes and Gregory M. Hulbert. Space-time finite element methods for elastodynamics: Formulations and error estimates. Computer Methods in Applied Mechanics and Engineering, 66(3):339 363, 1988.
- [21] Thomas J.R. Hughes, Leopoldo P. Franca, and Gregory M. Hulbert. New finite element formulation for computational fluid dynamics: Viii. the galerkin/least-squares method for advective-diffusive equations. Computer Methods in Applied Mechanics and Engineering, 73(2):173 189, 1989.
- [22] S.R. Idelsohn and E. Onate. Finite volumes and finite elements: Two 'good friends'. *International Journal for Numerical Methods in Engineering*, 37(19):3323 3341, 1994.
- [23] S.R. Idelsohn, E. Onate, and F. Del Pin. A lagrangian meshless finite element method applied to fluid-structure interaction problems. *Computers and Structures*, 81(8-11):655 671, 2003.
- [24] Ellen Kock and Lorraine Olson. Fluid-structure interaction analysis by the finite element method. a variational approach. *International Journal for Numerical Methods in Engineering*, 31(3):463 491, 1991.
- [25] C. Michler, S.J. Hulshoff, E.H. van Brummelen, and R. de Borst. A monolithic approach to fluid-structure interaction. *Computers and Fluids*, 33(5-6):839 848, 2004.
- [26] B. Nayroles, G. Touzot, and P. Villon. Generalizing the finite element method:
 Diffuse approximation and diffuse elements. Computational Mechanics, 10(5):307

 318, 1992.
- [27] C. Nitikitpaiboon and K.J. Bathe. Arbitrary lagrangian-eulerian velocity potential formulation for fluid-structure interaction. *Computers and Structures*, 47(4-5):871 891, 1993.
- [28] Lorraine G. Olson and Klaus-Juergen Bathe. Analysis of fluid-structure interactions. a direct symmetric coupled formulation based on the fluid velocity potential. *Computers and Structures*, 21(1-2):21 32, 1985.
- [29] K. C. Park, C. A. Felippa, and J. A. DeRuntz. Stabilization of staggered solution procedures for fluid-structure interaction analysis. *American Society of Mechanical Engineers*, *Applied Mechanics Division*, *AMD*, 26:95 124, 1977.
- [30] A.K. Slone, C. Bailey, and M. Cross. Dynamic solid mechanics using finite volume methods. *Applied Mathematical Modelling*, 27(2):69 87, 2003.

- [31] A.K. Slone, K. Pericleous, C. Bailey, M. Cross, and C. Bennett. A finite volume unstructured mesh approach to dynamic fluid-structure interaction: An assessment of the challenge of predicting the onset of flutter. *Applied Mathematical Modelling*, 28(2):211 239, 2004.
- [32] M. Souli, A. Ouahsine, and L. Lewin. Ale formulation for fluid-structure interaction problems. Computer Methods in Applied Mechanics and Engineering, 190(5-7):659 675, 2000.
- [33] Theodore Sussman and Jan Sundqvist. Fluid-structure interaction analysis with a subsonic potential-based fluid formulation. *Computers and Structures*, 81(8-11):949 962, 2003.
- [34] T.E. Tezduyar, M. Behr, and J. Liou. New strategy for finite element computations involving moving boundaries and interfaces. the deforming-spatial-domain/space-time procedure. i. the concept and the preliminary numerical tests. Computer Methods in Applied Mechanics and Engineering, 94(3):339 351, 1992.
- [35] Xiaodong Wang and Klaus-Jurgen Bathe. Displacement/pressure based mixed finite element formulations for acoustic fluid-structure interaction problems. *International Journal for Numerical Methods in Engineering*, 40(11):2001 2017, 1997.
- [36] Hou Zhang, Xiaoli Zhang, Shanhong Ji, Yanhu Guo, Gustavo Ledezma, Nagi Elabbasi, and Hugues DeCougny. Recent development of fluid-structure interaction capabilities in the adina system. Computers and Structures, 81(8-11):1071 1085, 2003.

		1
		j

